Exploring the protective mechanisms of insulin receptor substrate-1 under conditions of hypoxic-ischemic injury

Inauguraldissertation
zur Erlangung des Grades eines Doktors der Medizin
des Fachbereichs Medizin
der Justus-Liebig-Universität Gießen

vorgelegt von Taoli Lu

Aus Chengdu China

Gießen 2025

Aus dem Fachbereich Medizin der Justus-Liebig-Universität Gießen

Universitätsklinikum Gießen und Marburg, Standort Gießen
Medizinisches Zentrum für Neurologie

Neurologische Klinik

Experimentelle Neurologie

Gutachter: Prof. Dr. med. Thorsten R. Döppner

Gutachter: Prof. Dr. med. Eberhard Uhl

Tag der Disputation: 23.3.2026

INHALTSVERZEICHNIS

Seite

1 INTRODUCTION

1.1 Ischemic stroke

Stroke is a life-threatening medical condition and a major global public health challenge, characterized by a sudden disruption of cerebral blood flow, leading to neuronal damage and functional impairment (Barthels and Das 2020; Gil-Garcia et al. 2022; Balami et al. 2013; Zhu et al. 2024; Katan and Luft 2018). It can be classified into two main types: ischemic stroke and hemorrhagic stroke. Ischemic stroke accounts for approximately 85% of all cases and results from arterial stenosis or occlusion leading to hypoxia Hemorrhagic stroke, which includes intracerebral hemorrhage (ICH) and subarachnoid hemorrhage (SAH), both caused by the rupture of cerebral blood vessels (Turnbull et al. 2019; Gil-Garcia et al. 2022). Depending on the affected brain region the stroke symptoms vary, but commonly include aphasia, hemiparesis, visual disturbances, reduced consciousness, and headaches (Majumder 2024). The risk factors for stroke are classified as modifiable (e.g., hypertension, diabetes, hyperlipidemia, smoking, and sedentary lifestyle) and non-modifiable (e.g., age, sex, genetic predisposition) (Barthels and Das 2020; Katan and Luft 2018). Ischemic stroke is a leading cause of long-term disability, imposing substantial economic and social burdens, with millions of disability-adjusted life years (DALYs) lost annually (Balami et al. 2013; Wafa et al. 2020).

The etiology of ischemic stroke is multifactorial, involving several distinct mechanisms, including large-artery atherosclerosis, cardioembolism, small vessel disease, and less common causes. Large-artery atherosclerosis occurs when lipid-rich plaques and inflammatory cells accumulate in cerebral arteries, leading to narrowing or rupture, which can obstruct blood flow (Hankey 2013; Tsao et al. 2023). Cardioembolic stroke arises from thrombi that originate in the heart, often due to conditions like atrial fibrillation or valvular heart disease (Hankey 2013; Katan and Luft 2018; Zhu et al. 2024). Small vessel disease affects deep brain structures due to chronic hypertension and diabetes, leading to lacunar infarctions (Donnan et al. 2008; Hisham and Bayraktutan 2013). Less common causes include arterial dissection, hypercoagulable states, and congenital abnormalities such as patent foramen ovale (PFO), which can contribute to ischemic events (Anrather and Iadecola 2016; Donnan et al. 2008). Understanding these mechanisms is crucial for stroke prevention and management.

Current treatment strategies primarily focus on restoring cerebral perfusion, including intravenous thrombolysis with recombinant tissue plasminogen activator (rt-PA) and mechanical

thrombectomy. However, these interventions are constrained by a narrow therapeutic window, risk of hemorrhagic complications, and limited accessibility (Bai et al. 2019; Balami et al. 2013; Zhu et al. 2019). Despite advancements in acute stroke management, many patients continue to experience residual neurological deficits, underscoring the urgent need for safer and more effective therapeutic approaches. Addressing these challenges requires a deeper understanding of stroke pathophysiology and the development of novel neuroprotective strategies to enhance post-stroke recovery.

1.2 Pathophysiology of ischemic stroke

Stroke is a complex condition with evolving pathophysiology that leads to neuronal damage and functional deficits. It triggers a cascade of primary and secondary events—including energy failure, excitotoxicity, calcium overload, oxidative stress, apoptosis, BBB disruption, and inflammation—collectively known as the ischemic cascade. (Durukan and Tatlisumak2007).

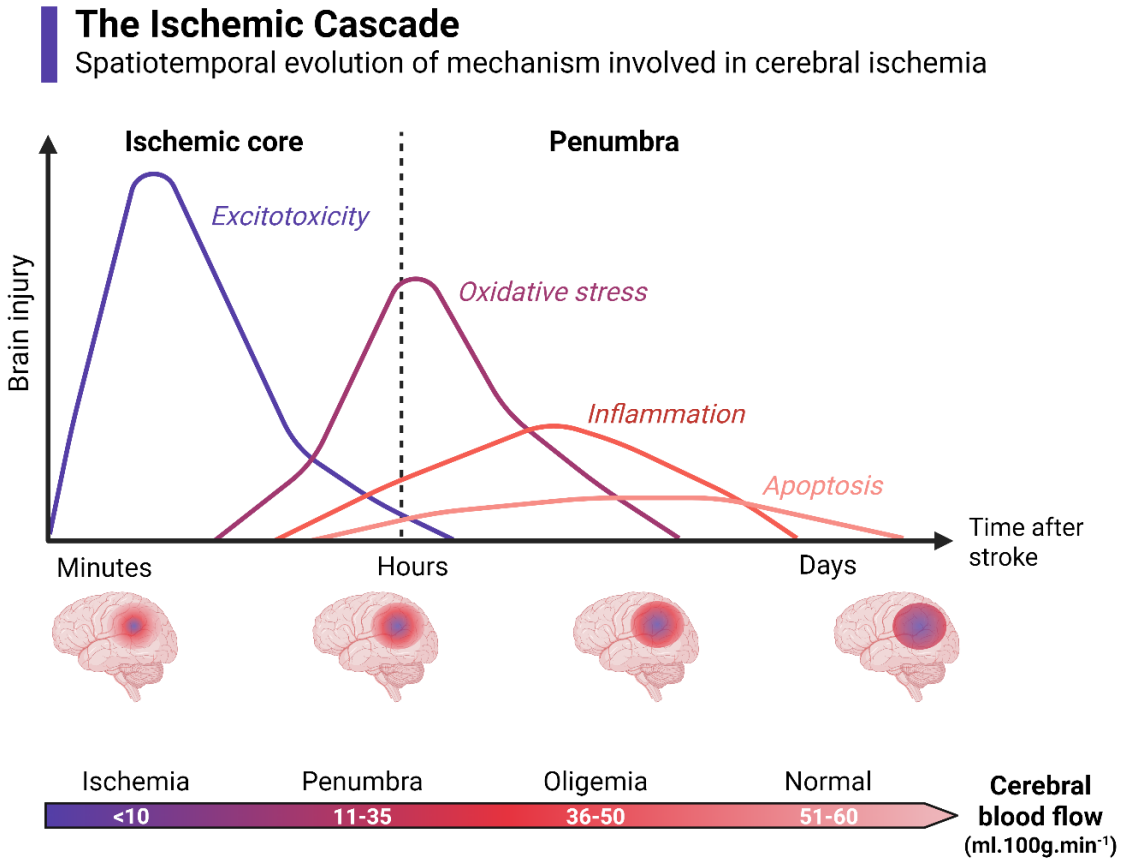

Figure 1. The Pathophysiology of stroke. This figure illustrates the time-dependent pathological processes following cerebral ischemia. Excitotoxicity occurs rapidly within minutes, followed by oxidative stress, inflammation, and apoptosis which develop over hours to days after stroke. The lower panel represents corresponding brain regions with varying cerebral blood flow (CBF). Figure created in Biorender.

1.2.1 Primary injury and energy failure

In the early minutes following ischemia, the interruption of cerebral blood flow leads to hypoxia and a shift in mitochondrial energy metabolism from aerobic to anaerobic pathways. Glucose is metabolized to lactic acid, resulting in acidosis. However, anaerobic metabolism is significantly less efficient, producing ATP at only 1/18th the efficiency of aerobic oxidation (Muthaian, Minhas, and Anand 2012). This energy failure disrupts ionic gradients, depolarizes neuronal membranes, and initiates the release of excitatory amino acids (EAA), particularly glutamate.

1.2.2 Excitotoxicity and calcium overload

The "excitotoxicity theory" suggests that the overactivation of glutamate receptors on postsynaptic membranes, such as N-Methyl-D-Aspartate receptor (NMDA) and (α-Amino-3-hydroxy-5-methyl -4-isoxazolepropionic acid receptor) AMPA receptors, contributes significantly to neuronal injury (Shen et al. 2022). Astrocytes release glutamate during ischemia, further exacerbating synaptic transmission and neuronal damage (Yang et al. 2019). The excessive activation of glutamate receptors leads to increased calcium influx into neurons. This intracellular calcium overload disrupts cellular homeostasis, activates harmful enzymatic pathways, and induces neuronal degeneration and death (Kristian 2004; Verma, Lizama, and Chu 2022).

1.2.3 Oxidative stress and free radical accumulation

Under normal physiological conditions, free radicals are tightly regulated by antioxidant systems, including superoxide dismutase, catalase, and peroxidase, which neutralize their harmful effects (Pham-Huy, He, and Pham-Huy 2008). However, ischemia disrupts this balance, leading to the accumulation of oxygen-free radicals. These free radicals react with polyunsaturated fatty acids (PUFAs) in cell membranes, initiating lipid peroxidation. Additionally, they promote oxidative damage to DNA, RNA, and proteins, contributing to neuronal injury and cell death (Sun et al. 2018; Veno, Schmidt, and Bork 2019).

1.2.4 Inflammation and BBB disruption

Following ischemic injury, damaged brain cells release pro-inflammatory cytokines, including tumor necrosis factor-α (TNF-α), interleukin-1 (IL-1), and platelet-activating factor (PAF). These molecules trigger an inflammatory response, increasing the expression of adhesion molecules on endothelial cells, allowing immune cells to cross the BBB and infiltrate the brain

parenchyma (Anrather and Iadecola 2016; Chamorro et al. 2016; Iadecola, Buckwalter, and Anrather 2020). This inflammation exacerbates neuronal damage and promotes secondary injury.

1.2.5 Secondary damage and long-term consequences

Over time, the secondary damage caused by inflammation, oxidative stress, and apoptosis contributes to progressive neuronal loss and functional deficits (Chamorro et al. 2016). Despite the brain's attempts at endogenous protection through neurotrophic factors and survival signaling pathways, the repair processes are often insufficient to fully recover from the damage (Kunz, Dirnagl, and Mergenthaler 2010). In the later stages, neuroplasticity, regeneration, and repair mechanisms attempt to restore some degree of function, but long-term complications, including gliosis and chronic inflammation, often persist (Yang et al. 2019). So, further research is needed to develop therapeutic strategies targeting multiple stages of this cascade to improve stroke outcomes.

1.3 The structure of insulin receptor substrate-1 (IRS-1)

The biological effects of insulin are mediated by its interaction with insulin receptors on the cell surface. The insulin receptor (IR), a ligand-activated tyrosine kinase, undergoes autophosphorylation upon insulin binding, phosphorylating intracellular substrates such as the insulin receptor substrate (IRS) family and Shc proteins (Nystrom and Quon 1999; Saltiel and Kahn 2001). IRS proteins, key mediators of insulin signaling, include four isoforms: IRS-1, IRS-2, IRS-3, and IRS-4. IRS-1, the first identified and most widely expressed isoform, is abundant in skeletal muscle, while IRS-2 is primarily expressed in the liver and pancreatic β cells (Chakraborty, Agoramoorthy, and Hsu 2011). IRS-1 features a pleckstrin homology (PH) domain and a phosphotyrosine-binding (PTB) domain, facilitating its interaction with the IR (Frendo-Cumbo 2021). Upon phosphorylation, IRS-1 serves as a key docking platform for downstream effectors, linking insulin receptor activation to multiple intracellular signaling pathways. Through these interactions, IRS-1 plays a crucial role in mediating insulin’s metabolic effects, including glucose uptake, glycogen synthesis, lipid metabolism, and protein synthesis.

Actually, the insulin signaling pathway constitutes a highly complex network, encompassing multiple feedback loops, interactions between major signaling branches, and cross-talk with

different receptor signaling pathways (Sedaghat, Sherman, and Quon 2002). However, it is generally recognized that the Phosphoinositide 3-kinase (PI3K) -dependent pathway is the primary insulin signaling branch regulating metabolic functions, while the Ras/Raf/mitogen-activated protein kinase (MAPK) pathway primarily contributes to the mitogenic and proliferative effects of insulin (Kim et al. 2006).

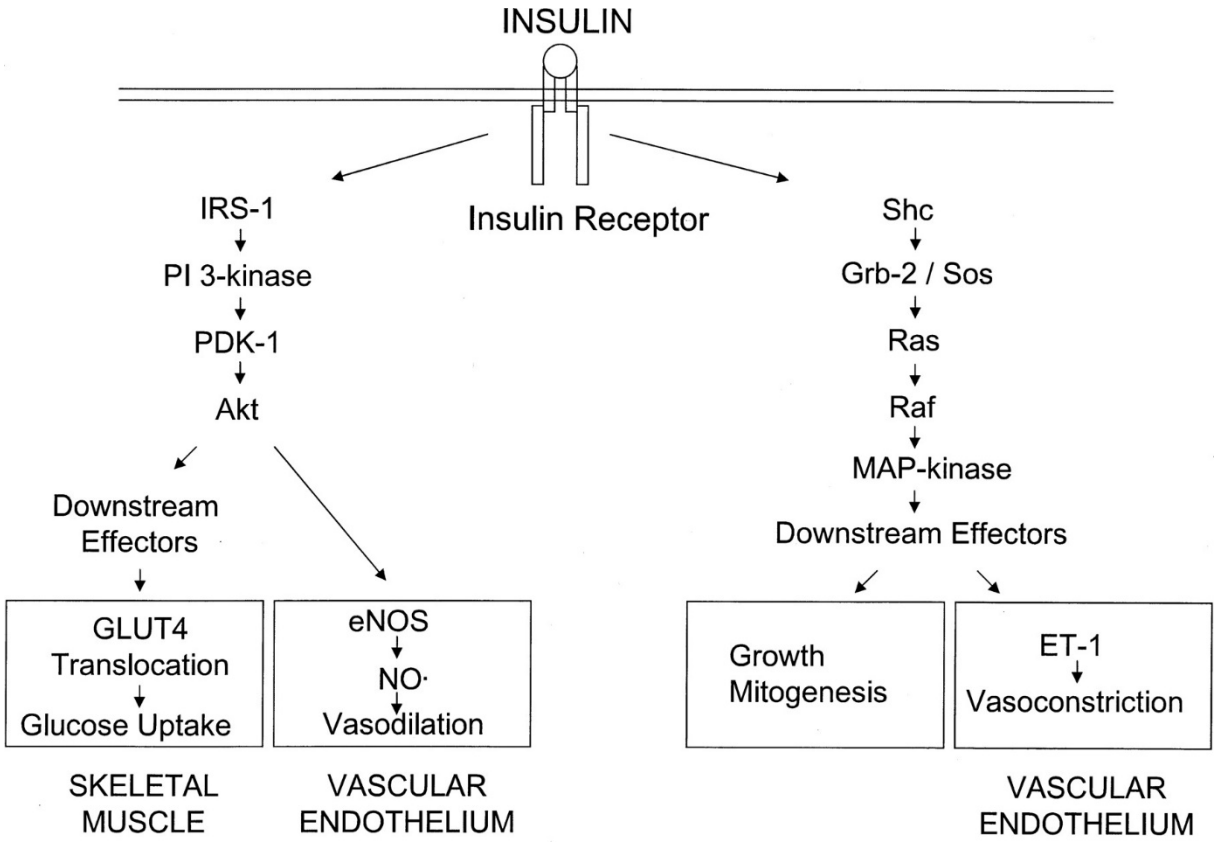

Figure 2. General features of insulin signal transduction pathways. This diagram illustrates two major signaling cascades activated by insulin or TGF-1 binding to the insulin receptor. The IRS-1/PI3K/PDK1/Akt pathway regulates metabolic and vascular effects, including GLUT4-mediated glucose uptake in skeletal muscle and eNOS-derived nitric oxide (NO) production leading to vasodilation in vascular endothelium. In parallel, the Shc/Grb2/Sos/Ras/Raf/MAPK pathway mediates mitogenic effects, including cell growth and ET-1–induced vasoconstriction in vascular endothelial cells. These coordinated pathways contribute to both metabolic regulation and vascular homeostasis. This figure is reproduced with permission from Kim JA et al.(Kim et al. 2006), Circulation, 2006;113(15):1883–1901. © 2006 Wolters Kluwer Health, Inc. License number: 6042511460637.

1.4 Regulation of IRS-1 by phosphorylation

1.4.1 Activation of IRS-1 by tyrosine phosphorylation

IRS-1 contains multiple phosphorylation sites that are crucial for its regulatory functions (Tanti et al. 1994; White 1997). Upon binding to the IR, IRS-1 undergoes tyrosine phosphorylation at

specific residues, creating docking sites for Src homology 2 (SH2) domain-containing proteins involved in downstream insulin signaling. Notably, phosphorylation at Y608 and Y628 of IRS-1 is critical, as these residues serve as binding sites for the p85 regulatory subunit of PI3K, thereby facilitating PI3K activation (Aguirre et al. 2000; Copps and White 2012; Li et al. 2007) Tyrosine-phosphorylated IRS-1 recruits PI3K through its SH2 domain, leading to the conversion of Phosphatidylinositol 4,5-bisphosphate (PIP2) into Phosphatidylinositol 4,5-bisphosphate (PIP3). This lipid second messenger facilitates the membrane recruitment of 3-Phosphoinositide-dependent protein kinase-1 (PDK1), enabling it to phosphorylate and activate protein kinase B (Akt). Activated Akt regulates several metabolic and cellular processes, including glucose uptake via GLUT4 translocation, glycogen synthesis through GSK-3β inhibition, and protein synthesis via mTOR signaling (Aguirre et al. 2000; Copps and White 2012; Li et al. 2007). In addition to the PI3K/Akt pathway, tyrosine-phosphorylated IRS-1 interacts with Grb-2 and Sos, triggering Ras activation and subsequently initiating the Raf/MEK/ERK signaling cascade. This pathway plays a key role in cell proliferation, differentiation, and survival, linking insulin signaling to mitogenic responses (Schinner et al. 2005; White 1997). In summary, IRS-1 tyrosine phosphorylation serves as a core in insulin signaling, regulating glucose metabolism, protein synthesis, cell survival, and mitogenic responses. Disruptions in this phosphorylation cascade contribute to insulin resistance and metabolic disorders, highlighting its critical physiological role.

1.4.2 Inhibition of IRS-1 by serine/threonine phosphorylation

IRS-1 contains over 50 potential serine/threonine phosphorylation sites, which play a crucial role in regulating insulin signaling. While some serine/threonine phosphorylations enhance or sustain IRS-1 activity, the majority act as negative regulators by impairing tyrosine phosphorylation, altering IRS-1 subcellular localization, or promoting its degradation (Copps and White 2012; Tanti and Jager 2009). In insulin-resistant tissues such as skeletal muscle, adipose tissue, and liver, IRS-1 exhibits increased serine phosphorylation, leading to a reduction in tyrosine phosphorylation and a subsequent decline in IRS-1 protein levels (Gual, Le Marchand-Brustel, and Tanti 2005; Schinner et al. 2005). This process is often mediated by kinases such as JNK, IKKβ, and mTOR, or by inflammatory cytokines such as TNF-α, which contribute to insulin resistance (Hotamisligil et al. 1996; Zhang et al. 2008). Key inhibitory phosphorylation sites include Ser307 (Ser312 in humans), Ser612, and Ser636/639, which interfere with IRS-1's ability to interact with the insulin receptor and PI3K (Aguirre et al. 2000; Li et al. 2007). Studies

in transgenic mice with serine-to-alanine mutations at specific phosphorylation sites demonstrate improved protection against high-fat diet-induced insulin resistance, further supporting the inhibitory role of serine phosphorylation in insulin signaling dysregulation (Morino et al. 2008). Overall, serine phosphorylation of IRS-1 is a key molecular mechanism underlying obesity- and diabetes-associated insulin resistance, highlighting its importance as a potential therapeutic target for metabolic disorders.

1.5 Regulation of IRS-1 by degradation

IRS-1 is a key adaptor protein in insulin signaling, and its degradation plays a crucial role in regulating cellular responses to insulin. IRS-1 degradation occurs through two primary pathways: autophagy-mediated degradation and proteasomal degradation via ubiquitination.

1.5.1 Autophagy-mediated degradation of IRS-1

Autophagy is a crucial cellular process for maintaining homeostasis by degrading and recycling damaged organelles and proteins. It plays a significant role in regulating IRS-1 levels, particularly under conditions of nutrient deprivation, hypoxia, or cellular stress, which activate autophagic pathways. IRS-1 degradation through autophagy involves recognition by adaptor proteins like p62/SQSTM1 (Bjorkoy et al. 2005; Pankiv et al. 2007). p62 contains domains that interact with ubiquitinated IRS-1 and autophagosomal protein microtubule-associated protein 1 light chain 3 (LC3) (Kraft, Peter, and Hofmann 2010). Specifically, p62's SH2 domain binds to phosphotyrosine (YXXM) motifs on IRS-1 (e.g., Tyr-608, Tyr-628, and Tyr-658), a mechanism similar to the binding of IRS-1 with the p85 subunit of PI3K (Geetha et al. 2012). This interaction ensures the specificity of IRS-1 sequestration into autophagosomes, double-membraned vesicles that subsequently fuse with lysosomes for proteolytic degradation.
Under starvation conditions, such as a lack of glucose, amino acids, and serum, autophagy selectively degrades IRS-1 without affecting the IR or Akt (Igawa et al. 2019). This degradation disrupts insulin signaling, as IRS-1 plays a pivotal role in the pathway. Interestingly, inhibition of autophagy or suppression of autophagy-related genes (e.g., ATG5, ATG16L1) prevents IRS-1 degradation and increases insulin-stimulated Akt phosphorylation ('Identification of New IRS1 Interactors in the Regulation of Insulin Signalling and Cell Proliferation'). Increased autophagy under stress conditions, such as hypoxia or ischemia, can result in excessive IRS-1 degradation. This contributes to disrupted insulin signaling, leading to insulin resistance and associated disorders, including neuronal dysfunction and metabolic diseases.

1.5.2 Ubiquitination-mediated degradation of IRS-1

The ubiquitin-proteasome system (UPS) is responsible for the selective degradation of IRS-1 through K48-linked polyubiquitination, targeting it for 26S proteasome degradation. Ubiquitin E3 ligase plays an important role in this process， including suppressor of cytokine signalling1 (SOCS1), SOCS3 (Rui et al. 2002), Cullin 7 (CUL7) (Xu et al. 2008), CLR7 (Xu et al. 2012), Cbl-b (Nakao et al. 2009), involved in the regulation of insulin resistance under various conditions. SOC proteins, particularly SOCS1/SOCS3, directly bind to IRS-1, facilitating its polyubiquitination and subsequent degradation. This mechanism is often upregulated in response to inflammatory cytokines, linking inflammation to insulin resistance (Rui et al. 2002). IRS-1 is also a proteolytic target of the Cullin 7 (CUL7) E3 ubiquitin ligase complex. In Cul7-deficient ($Cul7^{-/-}$) mouse embryonic fibroblasts, IRS-1 accumulates, underscoring the crucial role of the CUL7 E3 ubiquitin ligase in regulating IRS-1 degradation (Xu et al. 2008). Additionally, the Cullin-RING E3 ubiquitin ligase 7 (CRL7) mediates the ubiquitination of hyperphosphorylated IRS-1 (Xu et al. 2012). In skeletal muscle, unloading stress leads to atrophy through the induction and activation of the ubiquitin ligase Cbl-b. Upon induction, Cbl-b interacts with and degrades IRS-1, a key intermediate in IGF-1 signaling. This Cbl-b-dependent degradation of IRS-1 is mediated by ubiquitination (Nakao et al. 2009). Furthermore, serine phosphorylation of IRS-1, particularly at residues S636/639, S307, and S312, serves as a prerequisite for its ubiquitination. These phosphorylation events create recognition motifs for E3 ligases, facilitating subsequent ubiquitination and degradation (Wainszelbaum et al. 2012; Yoneyama et al. 2018). Under specific conditions, such as impaired autophagy, the Kelch-like proteins KLHL9 and KLHL13 form a complex with Cullin 3 (CUL3). This E3 ubiquitin ligase complex recognizes and ubiquitinates IRS-1, promoting its degradation (Dhanoa et al. 2013; Frendo-Cumbo et al. 2019).

Understanding the molecular mechanisms governing IRS-1 ubiquitination opens avenues for therapeutic interventions aimed at modulating this process. Inhibitors targeting specific E3 ligases or kinases responsible for IRS-1 phosphorylation could potentially restore normal insulin signaling in insulin-resistant states.

1.6 The role of IRS-1 in ischemic stroke: metabolic regulation and neuroprotection

The brain, an insulin-sensitive organ, expresses insulin receptors abundantly in the cerebral cortex, hippocampus, and cerebellum, highlighting the importance of insulin signaling in cognitive function and neuroprotection (Huang, Lee, and Hsu 2010; Schulingkamp et al. 2000). IRS-1 is a crucial mediator of insulin and IGF-1 signaling in the CNS, playing a fundamental role in neuronal metabolism, survival, and synaptic plasticity through pathways such as PI3K/Akt/mTOR and MAPK/ERK (Huang, Lee, and Hsu 2010; Schulingkamp et al. 2000; Shaw 2011).

1.6.1 IRS-1, glucose metabolism, and mitochondrial function in ischemic stroke

IRS-1 plays a pivotal role in neuronal glucose metabolism and mitochondrial function, primarily by activating the PI3K/Akt/mTOR pathway. Upon phosphorylation, IRS-1 facilitates GLUT4 translocation, ensuring efficient neuronal glucose uptake, which is essential for synaptic transmission, neurotransmitter release, and neuronal survival (Kleinridders et al. 2014; Milstein and Ferris 2021; van der Heide et al. 2005). Proper IRS-1 function supports mitochondrial ATP production, while its dysfunction leads to impaired glucose utilization, increased oxidative stress, and energy failure (Koepsell 2020).

In ischemic stroke, the loss of glucose and oxygen supply severely disrupts mitochondrial homeostasis, leading to excessive reactive oxygen species (ROS) generation and neuronal damage (Liu et al. 2018). IRS-1 dysfunction exacerbates these metabolic deficits, making neurons more vulnerable to ischemic injury. Enhancing IRS-1 signaling may serve as a therapeutic approach to improve mitochondrial resilience and protect against ischemic stroke-induced neuronal damage.

1.6.2 IRS-1 and autophagy regulation in ischemic stroke

Autophagy is a vital cellular process responsible for degrading and recycling damaged organelles and misfolded proteins, maintaining neuronal homeostasis. Insulin signaling, particularly through the IRS-1/PI3K/Akt/mTOR pathway, is a key regulator of autophagic activity in the CNS (Tramutola et al. 2015). Disruptions in IRS-1 signaling can impair autophagic flux, as observed in neurodegenerative diseases such as Alzheimer's and Parkinson's disease, where protein aggregation leads to neuronal dysfunction (Burillo et al. 2021; de Mello et al. 2019; Sekar and Taghibiglou 2018).

In ischemic stroke, autophagy has a dual role: it can be protective by removing damaged cellular components, but excessive activation may contribute to neuronal death (Carloni, Buonocore, and Balduini 2008; Galluzzi et al. 2016). Post-stroke oxidative stress and inflammation may further influence IRS-1 function and its regulatory role in autophagy. Recent studies indicate that IRS-1 activation can prevent excessive autophagy, reduce infarct size, and improve functional recovery by maintaining cellular homeostasis (Fu et al. 2023; Zang et al. 2023). Targeting IRS-1 signaling may provide new therapeutic strategies to modulate autophagy and protect against ischemic injury.

1.6.3 IRS-1 as a neurovascular modulator in ischemic stroke

Beyond neuronal protection, IRS-1 also plays a role in the neurovascular unit. Experimental models suggest that IRS-1 modulation influences BBB integrity, with contrasting effects depending on cell type. Neuronal IRS-1 activation is neuroprotective, reducing apoptotic markers like cleaved caspase-3 and Poly (ADP-ribose) polymerase (PARP) while maintaining BBB integrity. In contrast, excessive endothelial IRS-1 expression has been linked to increased vascular permeability, BBB dysfunction, and worsened neurovascular damage (Tu et al. 2021; Tu et al. 2016).

These findings suggest that IRS-1's role in ischemic stroke is complex and cell-type-specific. While enhancing neuronal IRS-1 function may provide neuroprotection, uncontrolled IRS-1 activation in endothelial cells could have detrimental effects on the BBB. Understanding this dual role is essential for developing targeted therapeutic strategies that selectively modulate IRS-1 signaling in different cell populations to optimize stroke recovery.

1.7 Aim of the thesis

Despite growing evidence linking IRS-1 dysregulation to CNS diseases, the precise mechanisms by which IRS-1 contributes to ischemic stroke progression and recovery remain incompletely understood. This thesis primarily investigates the expression of IRS-1 after oxygen glucose deprivation (OGD; an in vitro stroke model) and its potential regulatory mechanisms. Additionally, it aims to explore the neuroprotective mechanisms of IRS-1 in ischemic stroke, with a particular focus on its role in metabolic regulation, autophagy, and neurovascular interactions. By elucidating these mechanisms, this study seeks to provide insights into the therapeutic potential of IRS-1 modulation for improving stroke outcomes and developing targeted treatment strategies.

2 MATERIALS AND METHODS

2.1 Lab materials

Table 1. Laboratory equipment used

Equipment	Manufacturer
Axio Scan Z1 Microscope	Zeiss, Germany
Biological Safety Cabinet	NuAire, USA
Biometra TPersonal Thermocycler	Analytik Jena, Germany
ChemoCam Imager (ECL System)	INTAS, Germany
EV 231 Power Supply	PEQLAB / Avantor, USA
Hanna edge® pH Meter	Hanna Instruments, USA
Universal 320R Centrifuge	Hettich, Germany
Inverted Microscope	A.KRÜSS Optronic, Germany
Mikro 120 Tabletop Centrifuge	Hettich, Germany
Multiskan EX Microplate Reader	Thermo Fisher, USA
MyCycle™ Thermal Cycler	Bio-Rad, USA
NanoPhotometer® P330	Implen, Germany
Neubauer Counting Chamber	Karl Hecht, Germany
Peristaltic Pump	Carl Roth, Germany
Pipettes & Multi-Dispensers	Eppendorf, Gilson, Sartorius (Germany/France)
QuantStudio™ 3 Real-Time PCR	Thermo Fisher, USA
Refrigerators and Freezers	Liebherr, Panasonic, Thermo Fisher
Roller RM5 Assistent 348	Karl Hecht, Germany
Vortex-Genie™ 2	Thermo Fisher, USA
Trans-Blot® SD System	Bio-Rad, USA
Water Bath	Memmert, Germany
Weighing Balances	Sartorius, Germany

Table 2. Lab consumables

Item	Manufacturer
Cell culture dish 60 x 15 mm	Sarstedt, Germany
Cell scraper	Greiner Bio-One, Germany
Cellstar® 6 well plate	Greiner Bio-One, Germany
Cellstar® 24 well plate	Greiner Bio-One, Germany
Flat bottom lid TC-Plate 96 well sterile	Greiner Bio-One, Germany
Cellstar® cell culture flask 25 cm²	Greiner Bio-One, Germany
Cellstar® cell culture flask 75 cm²	Greiner Bio-One, Germany
Falcon® 70 µm Cell Strainer	Corning, USA
Glass Pasteur pipettes 150 mm	BRAND, Germany
Microscope cover slips	Karl Hecht, Germany
Minisart® Syringe Filters (0.2 µm)	Sartorius, Germany
Mr. Frosty™ freezing container	Thermo Fisher, USA
PVDF membrane 0.45 µm	Thermo Fisher, USA
PVDF membrane 0.2 µm	Carl Roth, Germany
Parafilm®	Merck, Germany

Item	Manufacturer
Pipette tips (pyrogen and DNase free) 10 µl; 20 µl; 100 µl; 200 µl; 1000 µl	nerbe plus, Germany
Pipette tips standard 10 µl; 20 µl; 100 µl; 200 µl; 1000 µl	Sarstedt, Germany
Plastic feeding tubes 22ga 25mm, sterile	Instech, USA
Plastic pipettes: 5 ml; 10 ml; 25 ml	Greiner Bio-One, Germany
Cell culture dish 60 x 15 mm	Sarstedt, Germany
Cell scraper	Greiner Bio-One, Germany

Table 3. Chemical

Compound Name	Manufacturer
Ammonium persulfate (APS)	Carl Roth, Germany
B-27™ Supplement Gibco™	Thermo Fisher, USA
Bovine Serum Albumin (BSA)	Capricorn Scientific, Germany
Calcium Chloride($CaCl_2$)	Carl Roth, Germany
3-(4,5-Dimethyl-2-thiazolyl)-2,5-diphenyl-2H-tetrazolium Bromide (MTT)	Merck, Germany
4',6-Diamidino-2-phenylindol dihydrochloride (DAPI)	Thermo Fisher, USA
DMEM/Ham'sF-12 (DMEM/F-12)	Capricorn Scientific, Germany
Dipotassium phosphate (K_2HPO_4)	Carl Roth, Germany
Disodium phosphate (Na_2HPO_4)	Carl Roth, Germany
Dulbecco's Modified Eagle Medium (DMEM)/F-12 Gibco™	Thermo Fisher, USA
Dimethyl sulfoxide (DMSO)	Carl Roth, Germany
DNAse I	Merck, Germany
Dulbecco's phosphate buffered saline (DPBS) ROTI®Cell 10×	Carl Roth, Germany
Ethanol 100% Sigma-Aldrich®	Merck, Germany
Fetal bovine serum (FBS) Gibco™	Thermo Fisher, USA
Glucose	Carl Roth, Germany
Glycine	Merck, Germany
GlutaMAX™ Supplement	Thermo Fisher, USA
Hanks' Balanced Sait Solution (HBSS) (10×)	Thermo Fisher, USA
HEPES Buffer Solution(1M) Gibco™	Thermo Fisher, USA
HEPES powder	Merck, Germany
Hydrochloric acid 37% Sigma-Aldrich®	Merck, Germany

Table 4. Kits

Kits	Manufacturer	Cat.No	Method
DC Protein Assay Reagent	Bio-Rad, USA	5000113	Protein quantification
SuperSignal® West Pico Chemi-luminescent substrate	Thermo Fisher, USA	34580	Western Blot
Maxima H Minus First Strand cDNA-Synthese-Kit	Thermo Fisher, USA	K1652	Reverse Transcription
PowerUp™ SYBR™ Green Master Mix	Applied Biosystems, USA	A25776	Polymerase Chain Reaction (PCR)

Table 5. Buffer

Buffer Name	Ingredients	Amount
APS	H_2O APS	10 ml 1 g
Blocking buffer (5% BSA)	TBST BSA	100 ml 5 g
Running Buffer	H_2O SDS-PAGE 10×	1800 ml 200 ml
SDS solution	H_2O SDS	10 ml 1 g
TBS20×	H_2O NaCl Tris	1000 ml 175.4 g 48.2 g
TBST 1×	TBS 20× Tween H_2O	50 ml 1 ml 950 ml
Transfer Buffer	H_2O Methanol SDS-PAGE 10×	1400 ml 400 ml 200 ml
BSS0 10× stock solution	ddH_2O NaCl KCl $MgSO_4$ $NaH_2PO_4•H_2O$	800 ml 68 g 4 ml 2 g 1.4 g
BSS0 1× solution	ddH_2O 10× BSS0 1 M $NaHCO_3$ 1 M HEPES 30 mM Glycine 1 M $CaCl_2$	43 ml 50 ml 13.1 ml 5 ml 166 µl 900 µl
DPBS	ddH_2O DPBS	100 ml 900 ml
Poly-D-lysine (PDL)	DPBS Poly-D-lysine	100 ml 100 ml
Neurobasal medium	Neurobasal Medium (1×) B27 Supplement (2%) Transferrin (5 µg/ml) L-glutamine (0.5 mM) Pen-Strep (1%)	500 ml 10 ml 500 µl 250 µl 5 ml

Table 6. Primary Antibodies

Name	Host	Dilution	Method	Art.No	Manufactureer
IRS-1	Rabbit	1:1000	WB	2382	Cell Signaling
p-IRS-1$^{Ser636/639}$	Rabbit	1:1000	WB	2388	Cell Signaling
p-IRS-1^{Try612}	Rabbit	1:1000	WB	44-816G	Thermo Fisher
β-actin	Rabbit	1:1000	WB	ab8227	Abcam
IRS-1	Rabbit	1:200	IF	17509-1-AP	Proteintech
NeuN	Mouse	1:200	IF	MAB377	Millipore

Table 7. Second Antibodies

Name	Host	Dilution	Method	Art.No	Manufactureer
Goat Anti-Rabbit IgG H&L (HRP)	Goat	1:10000	WB	Ab6721	Abcam
Goat anti-Rabbit Alexa Fluor™ 488	Goat	1:500	IF	A11008	Cell Signaling
Goat anti-Mouse Alexa Fluor™ 555	Goat	1:500	IF	A21422	Thermo Fisher

2.2 Isolation of Primary Neurons

Primary neurons were prepared following the protocol from Thomas et al (Fath et al. 2009) with some modification. First, a 6-well plate was coated with 2 ml of 0.1 mg/ml poly-D-lysine (PDL) per well, while a 24-well plate was coated with 1 ml of PDL per well. The plates were then incubated at 37°C for at least 1 hour. After incubation, they were washed three times with double-distilled water (ddH_2O) and allowed to air dry before use.

Pregnant C57BL/6J mice (E16.5) were euthanized using isoflurane, and the embryos were carefully extracted from the uterus. The embryos were then decapitated, and their brains were removed from the skulls. After gently stripping away the meninges, the cerebral cortex and hippocampus were isolated and transferred to a 15 ml tube containing 8 ml of ice-cooled HBSS. The HBSS was subsequently removed, and the tissue was digested with 0.05% Neuron Isolation Enzyme for 20 minutes in a 37°C water bath, while shaking every 5 minutes. After digestion, 50 µl of DNase was added, and the mixture was incubated at room temperature (RT) for 1 minute. Digestion was terminated by adding 2 ml of neurobasal medium (components are shown in **Table 5**). The tissue was homogenized by pipetting 7-10 times with a polished Pasteur pipette. After waiting for 1 minute for the tissue to sink, the supernatant was transferred to a fresh 15 ml tube. An additional 1 ml of neurobasal medium was added to the remaining tissue, and the homogenization process was repeated. The supernatant was collected again and centrifuged at 800 rpm for 4 minutes and generated supernatant was discarded afterwards. The cell pellet was resuspended in 2 ml of neurobasal medium, and the cell number was counted using a Neubauer cell counting chamber. The cells were then seeded onto PDL pre-coated 6-well or 24-well plates containing neurobasal medium. The seeding density for the 6-well plate was 1×10^6 cells per well, while for the 24-well plate, it was 2×10^5 cells per well. The cultures were maintained under standard conditions (5% CO_2, 37°C). After 3-4 hours, the medium was replaced to remove debris. The primary neurons were then cultured for an additional 5-7 days before being used in subsequent experiments.

2.3 Oxygen-glucose deprivation (OGD) model

The primary neurons were cultured for 5-7 days until they reached a confluency of 80-90%. Upon reaching confluency, the cells were washed twice with DPBS to remove residual nutrients. The culture medium was replaced with an equal volume of glucose-free balanced salt solution (BSS0) (components are shown in **Table 5**). Following this the cells were transferred to the hypoxic chamber and incubated under hypoxic conditions (1.5% O_2, 5% CO_2, 45% humidity at 37°C) for a pre-determined time based on the experimental requirements. Afterwards, BSS0 was removed, and the cells were washed once with DPBS before adding neurobasal medium and incubating the cells for 24 hours of reoxygenation (RO) under standard conditions. After reoxygenation, the cells were subjected to various analyses, including cell viability assays, RNA isolation, protein extraction, and immunofluorescence staining, as required for further experimentation.

2.4 Cell viability assay

Primary neurons were seeded in a 24-well plate at a density of 2×10^5 cells per well in 1 ml of neurobasal medium. After 2 h, 4 h, 6 h, and 8 h OGD, the cells were subjected to 24 hours of RO. Then, 100 µl MTT solution (3-(4,5-dimethylthiazol-2-yl)-2,5-diphenyltetrazolium bromide) was added to each well to achieve a final working concentration of 0.5 mg/ml MTT and incubated for 3 h at 37°C. After incubation, the MTT solution was removed and replaced with 1 ml of dimethyl sulfoxide (DMSO). The plate was shaken on an orbital shaker at RT for 3-5 minutes to dissolve the formazan crystals. Thereafter, 200 µl of the dissolved solution from each well were transferred to a 96-well microtiter plate to measure the absorbance spectrophotometrically at 570 nm. Results were presented as a percentage of the control group, comparing normoxia vs. hypoxia conditions.

2.5 Immunofluorescence

PDL-coated coverslips were placed in a 24-well plate before seeding primary neurons at a density of 2×10^5 cells per well. The cells were then cultured for 3-5 days under standard conditions. Afterwards, the medium was removed, and the cells were washed three times with PBS for 5 minutes each time. For fixation, the coverslips were treated with 4% paraformaldehyde (PFA) for 10 minutes at RT and then washed three times with PBS. Permeabilization was performed by adding 0.25% PBS-Triton X-100 for 10 minutes at RT, followed by another three washes with PBS. To block non-specific binding, the coverslips were incubated with blocking solution

(5% Bovine Serum Albumin (BSA) dissolved in PBS) for 60 minutes at RT. The primary antibody was diluted in blocking solution according to the specification in (**Table 6**) and applied to the coverslips before incubating overnight at 4°C. The following day, the coverslips were washed three times with PBS before adding a fluorochrome-conjugated secondary antibody (**Table 7**). The cells were incubated for 1 hour at RT in the dark, then washed three times with PBS. DAPI staining solution (1:1000 dilution in PBS) was applied and incubated for 1 minute, followed by another three washes with PBS. Finally, the coverslips were embedded in anti-fade mounting medium on microscope slides and stored at 4°C overnight until visualization.

2.6 RNA isolation and quantitative real-time PCR analysis

2.6.1 Total RNA extraction

Total RNA was extracted when the cell confluence reached 90%, using the RNeasy Kit (QIAGEN, USA, **Table 4**) according to the manufacturer's instructions. Briefly, cells were lysed directly in the culture vessel by adding RLT Buffer (with 1% β-mercaptoethanol). Cell lysates were homogenized by pipetting thoroughly. An equal volume of 70% ethanol was added to the lysate, mixed thoroughly, and the mixture was transferred to an RNeasy Mini spin column placed in a 2 mL collection tube. Columns were centrifuged for 15 seconds at 8000 × g to bind RNA to the membrane. The flow-through was discarded. Columns were washed with 700 µL of RW1 Buffer and centrifuged for 15 seconds at 8000 × g. The sequential washes with 500 µL of RPE Buffer were performed, and the second wash centrifuged for 2 minutes to ensure the membrane was dry. The column was placed in a new 1.5 mL collection tube, and 30 µL of RNase-free water was added directly to the membrane. The RNA was eluted by centrifugation at 8000 × g for 1 minute. RNA concentration and purity were measured using a NanoPhotometer® P330 (Implen GmbH, München, Germany).

2.6.2 Reverse transcription

RNA was reversely transcribed to cDNA with the Maxima H Minus First Strand cDNA-Synthese-Kit (Thermo Scientific, USA, **Table 4**). Briefly, 1000 ng of template RNA was transcribed into cDNA in a total volume of 15 µl according to the manufacturer′s instructions (**Table 8**). All components were added to a sterile, nuclease-free tube, followed by a quick centrifugation and incubation at 65°C for 5 minutes. The tube was then chilled on ice, briefly centrifuged again, and kept on ice. Subsequently, the components listed in (**Table 9**) were carefully

added, and the mixture was incubated for 10 minutes at 25°C, followed by 15 minutes at 50°C, and the reaction was finally terminated by heating at 85°C for 5 minutes.

Table 8. First-Strand cDNA synthesis

Component	Volume
Template	1000 ng
Oligo (dT) 18 primer	0.25 µl
Random hexamer primer	0.25 µl
Nuclease-free water	Add to 15 µl

Table 9. First -Strand cDNA synthesis

Component	Volume
5 X RT Buffer	4 µl
Maxima H Minus Enzyme Mix	1 µl
Total volume	To 20 µl

2.6.3 Quantitative real-time PCR

Then qRT-PCR assay was applied with the PowerUp™ SYBR™ Green Master Mix kit (Applied Biosystems™, USA, Table 4) according to the manufacturer's instructions. In a total volume of 20 µl, the components were combined with the miRNA-specific forward primer and the universal reverse primer as stated in (**Table 10**). The reaction condition was carried out in accordance with the standard procedure (**Table 11**). All the primers were gifted by the Max Planck Institute for Heart and Lung Research (Bad Nauheim, Germany, **Table 12**). Relative mRNA expression was evaluated using the comparative ΔΔCT method (ΔCT= target gene - housekeeping gene; ΔΔCT = 2^-ΔCT) and β-actin was used as the housekeeping gene.

Table 10: Pipetting scheme for qRT-PCR

Table 10. Pipetting scheme for qRT-PCR

Component	Volume
PowerUp SYBR Green Master Mix	10 µl
Forward and reverse primer (500nM)	2 µl
dDNA template	2 µl
Nuclease-free water	6 µl

Table 11. Standard protocol for qRT-PCR reaction

Step	Temperatrue	Time	Cycle
Initial denaturation	95°C	2 minutes	1
Ampflication cycles Denaturation	95°C	15 seconds	40

Step	Temperatrue	Time	Cycle
Anneal/extend	60℃	1 minute	
Melt curve analysis Denaturation Anneal/extend Dissociation	 95℃ 60℃ 60℃-95℃	 15 seconds 1 minute 0.1℃ / sec	 1

Table 12. Primers

Primer	5-3 sequence
IRS-1	Forward GATCGTCAATAGCGTAACTG
	Reverse ATCGTACCATCTACTGAAGAG
actin	Forward AGCCATGTACGTAGCCATCC
	Reverse TCACAATGCCTGTGGTACG

2.7 Western blot analysis

2.7.1 Drug treatment

Primary neurons were seeded in a 6-well plate at a density of 1×10^6 cells per well until reaching 80-90% confluency. Prior to OGD, the cells were pretreated with 3-Methyladenine (3-MA), Rapamycin, MG132, or DMSO (vehicle control) for 1 hour. During OGD, the medium was replaced with BSS0 containing the same concentrations of the respective chemicals. Following OGD, the medium was replaced with neurobasal medium supplemented with the same concentrations of the respective chemicals for the RO phase, ensuring continuous treatment until protein extraction.

The optimal concentration of MG132 was determined by testing a range of concentrations (0.05 μM, 0.1 μM, 0.5 μM, 1 μM, and 5 μM). Cell viability at each concentration was evaluated using the MTT assay to identify a dose that maintained sufficient neuronal viability while exerting pharmacological effects. Based on these results, 0.05 μM MG132 was selected for subsequent experiments. 3-MA and rapamycin were dissolved in dimethyl sulfoxide (DMSO). For 3-MA, concentrations of 0.1 mM, 0.5 mM, 1 mM, 1.5 mM, and 2.5 mM were tested, while rapamycin was applied at 50 nM, 100 nM, 150 nM, and 200 nM. The optimal concentrations, determined based on MTT assay results evaluating cell viability, were 0.5 mM for 3-MA and 100 nM for rapamycin.

To ensure consistency and eliminate solvent-induced variability, all treatment groups were exposed to the same final DMSO concentration of 0.5%. This concentration was sufficient to dissolve the highest drug concentrations used and falls within the accepted non-toxic range for neuronal cell culture.

2.7.2 Protein extraction and quantification

Following the abovementioned treatment, the cells were washed twice with ice-cold PBS to remove residual medium and debris. Subsequently, adherent cells were scraped off using a cold plastic cell scraper and transferred into a pre-cooled 1.5 mL microcentrifuge tube. The cell suspension was centrifuged at 1200 × g for 5 minutes at 4°C, afterwards the supernatant was discarded. The cell pellet was lysed by adding RIPA buffer supplemented with 1% protease inhibitor cocktail and 0.1% phosphatase inhibitor. Then the lysate was incubated on ice for 30 minutes, and was thoroughly mixed by vortexing every 5 minutes to facilitate complete lysis. To further disrupt the cells, sonication was performed for 30 seconds on ice. The lysates were centrifuged at 12000 × g for 20 minutes at 4°C, and the supernatant, containing the extracted proteins, was collected and stored at -80°C for future analysis.

Protein concentrations were determined using the DC Protein Assay Kit (Bio-Rad Laboratories, CA, USA) according to the manufacturer's instructions. Briefly, a standard curve was prepared using BSA (0-1.4 μg/μL). Cell lysates and standards (5 μL) were mixed with 25 μL of Reagent A + S mixture in a 96-well plate, followed by the addition of 200 μL of Reagent B. After 15 minutes of incubation at RT, the absorbance was measured at 750 nm. Protein concentrations were calculated based on the standard curve, and all samples were adjusted to equal concentrations using RIPA buffer. Finally, samples were mixed with reducing loading buffer and heated at 95°C for 9 minutes to denature proteins before electrophoresis.

2.7.3 SDS-PAGE and Western blot

Equal amounts of protein (20-30 μg per lane) were loaded onto an 8% or 15% SDS-PAGE gel, depending on the molecular weight of the target proteins. Electrophoresis was carried out at 80 V for stacking gel separation. When the samples migrated into the separating gel, the voltage was increased to 120 V, and electrophoresis was continued until the bromophenol blue dye reached the bottom of the gel. Before transfer, the polyvinylidene fluoride (PVDF) membrane was activated by immersing it in methanol for 10 seconds. A transfer "sandwich" was assembled in the following order: filter paper, gel, PVDF membrane, and filter paper, ensuring the assembly was free of air bubbles. Protein transfer was performed using a semi-dry transfer system at 1.5 mA/cm² for 30 minutes. To prevent nonspecific binding, the PVDF membrane was blocked with 5% BSA dissolved in TBS-T for 1 hour at RT. The membrane was then incubated overnight at 4°C with primary antibodies diluted in blocking buffer (Table 6). The following day, after washing the membrane three times with TBS-T, it was incubated with

horseradish peroxidase (HRP)-conjugated secondary antibodies diluted 1:10,000 in blocking buffer for 1 hour at RT. After that, the membrane was washed three times with TBS-T. Finally, the membranes were immersed in an enhanced chemiluminescence (ECL) reagent before the blots were exposed to the imaging equipment INTAS ECL Chemostar (GmbH, Göttingen, Germany). Band intensities were quantified and analyzed using ImageJ software (NIH, USA).

2.8 Experiment design

Pregnant mice at embryonic day 16.5 (E16.5) were used to obtain embryos. Brains were dissected from the embryos and processed into cell suspensions to isolate primary neurons. The neurons were cultured and then subjected to OGD in a hypoxia chamber to mimic ischemic stroke conditions. After OGD, various assays including MTT assay for cell viability, fluorescence imaging, and Western blotting were performed to analyze cellular responses.

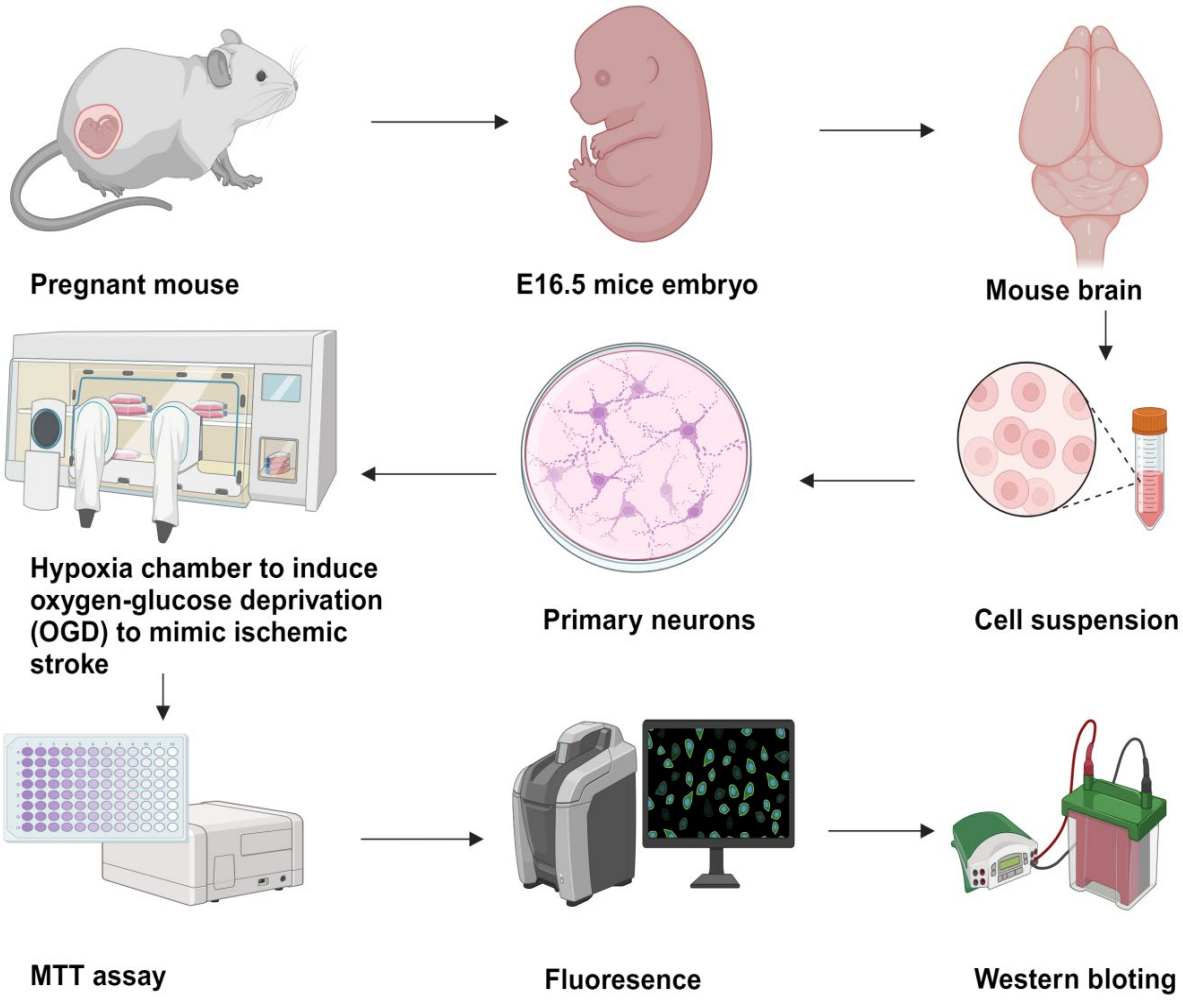

Figure 3. Schematic illustration of the experimental procedure. Figure created in Biorender.

2.9 Statistical analysis

For comparison of two groups, the two-tailed independent Student's t-test was used. For comparison of three or more groups, a one-way analysis of variance (ANOVA) followed by the Tukey's post-hoc-test was used. GraphPad Prism 10 software (GraphPad sofware, California, USA) was used for statistical analysis and generation of the graphs, whereas Excel was utilized for data collection. All data are given as mean ± standard deviation (SD), and p values less than 0.05 was considered significant.

3 RESULT

3.1 Isolation and characterization of primary neurons

The morphology of primary neurons was assessed using bright-field microscopy, revealing characteristic features by round soma and extended, branched neurites (**Figure 4**). To confirm neuronal identity, immunofluorescence staining was performed with the NeuN antibody, which targets the neuron-specific, DNA-binding protein NeuN, commonly expressed in the nuclei of mature neurons (**Figure 5**).

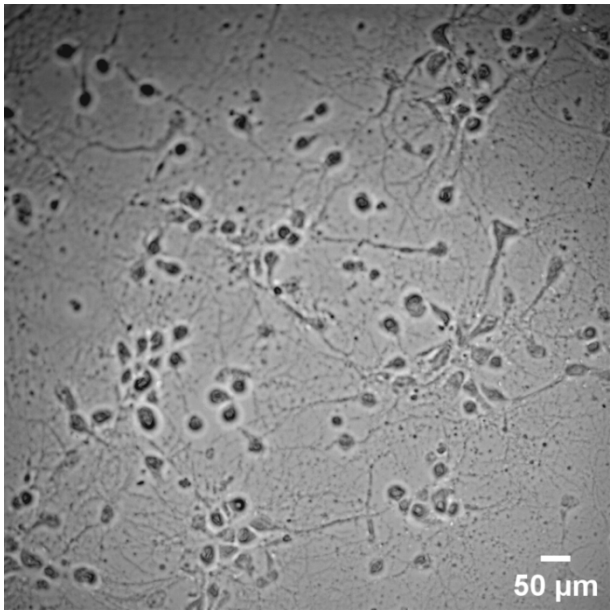

Figure 4. Morphology of primary neurons. Primary neurons were isolated from cerebral cortices and hippocampi of E16.5 mouse fetus.

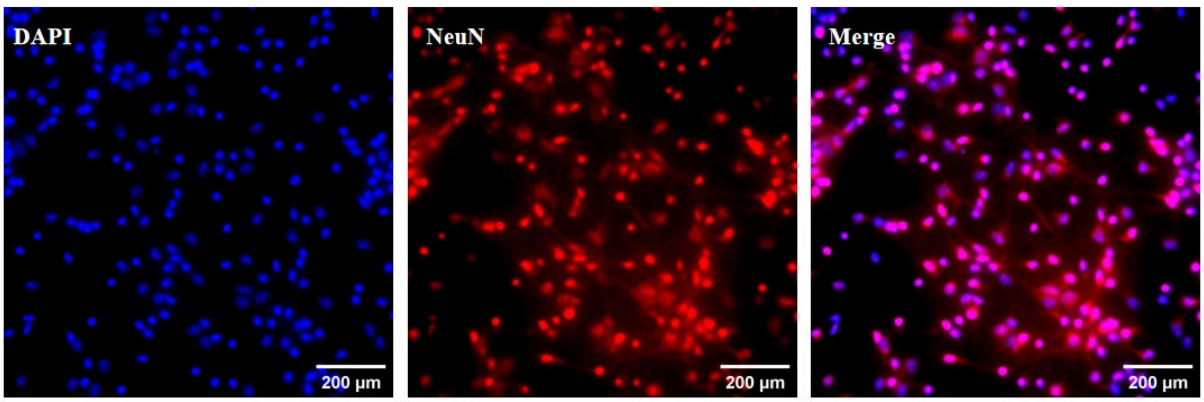

Figure 5. Identification of primary neurons. Immunofluorescence staining was performed to identify the primary neurons by the neuronal marker NeuN (Red). Blue indicates staining of cell nuclei by means of DAPI.

3.2 Establishment of an oxygen-glucose deprivation (OGD) model in vitro and IRS-1 expression in primary neurons under hypoxic conditions

Cell viability in primary neurons subjected to 2 h, 4 h, 6 h, and 8 h OGD followed by 24 h RO was assessed using the MTT assay. A normoxia group, which remained under standard culture conditions without OGD exposure, served as control. In total, five groups were analyzed: normoxia, 2 h, 4 h, 6 h, and 8 h of OGD (n = 6 per group). As shown in **Figure 6A**, a statistically significant reduction in cell viability was observed in all OGD groups compared to the control group ($p < 0.005$). Notably, exposure to 4 h of OGD followed by 24 h of RO resulted in approximately 50% cell viability, representing a moderate yet physiologically relevant level of neuronal injury. This condition provided an optimal balance between inducing cellular stress and preserving sufficient cell survival, and was therefore selected for subsequent molecular analyses.

To further investigate the effects of OGD on IRS-1 expression, RT-qPCR and Western blot analyses were performed to assess IRS-1 mRNA and protein levels, respectively. Based on the MTT assay findings, OGD durations of 2 h, 4 h, and 6 h followed by 24 h RO were selected for a detailed analysis. As shown in **Figure 6B**, a slight but non-significant reduction in IRS-1 mRNA expression was observed across the OGD-treated groups compared to the normoxia group ($p > 0.05$).

In contrast, Western blot analysis revealed a significant and progressive decrease in IRS-1 protein expression with increasing OGD duration. Compared to the normoxia control, IRS-1 protein levels were significantly reduced in the OGD 2 h / RO 24 h group ($p < 0.0001$), with further reductions observed in the OGD 4 h / RO 24 h and OGD 6 h / RO 24 h groups ($p < 0.0001$ for both; **Figure 6C, D**). These findings suggest that the OGD-induced downregulation of IRS-1 occurs primarily at the post-transcriptional level, potentially involving altered protein stability or degradation pathways. Among these conditions, the 4 h OGD / 24 h RO group demonstrated a clear reduction in IRS-1 protein expression while maintaining a moderate level of cell viability, supporting its use as a representative condition for further experiments.

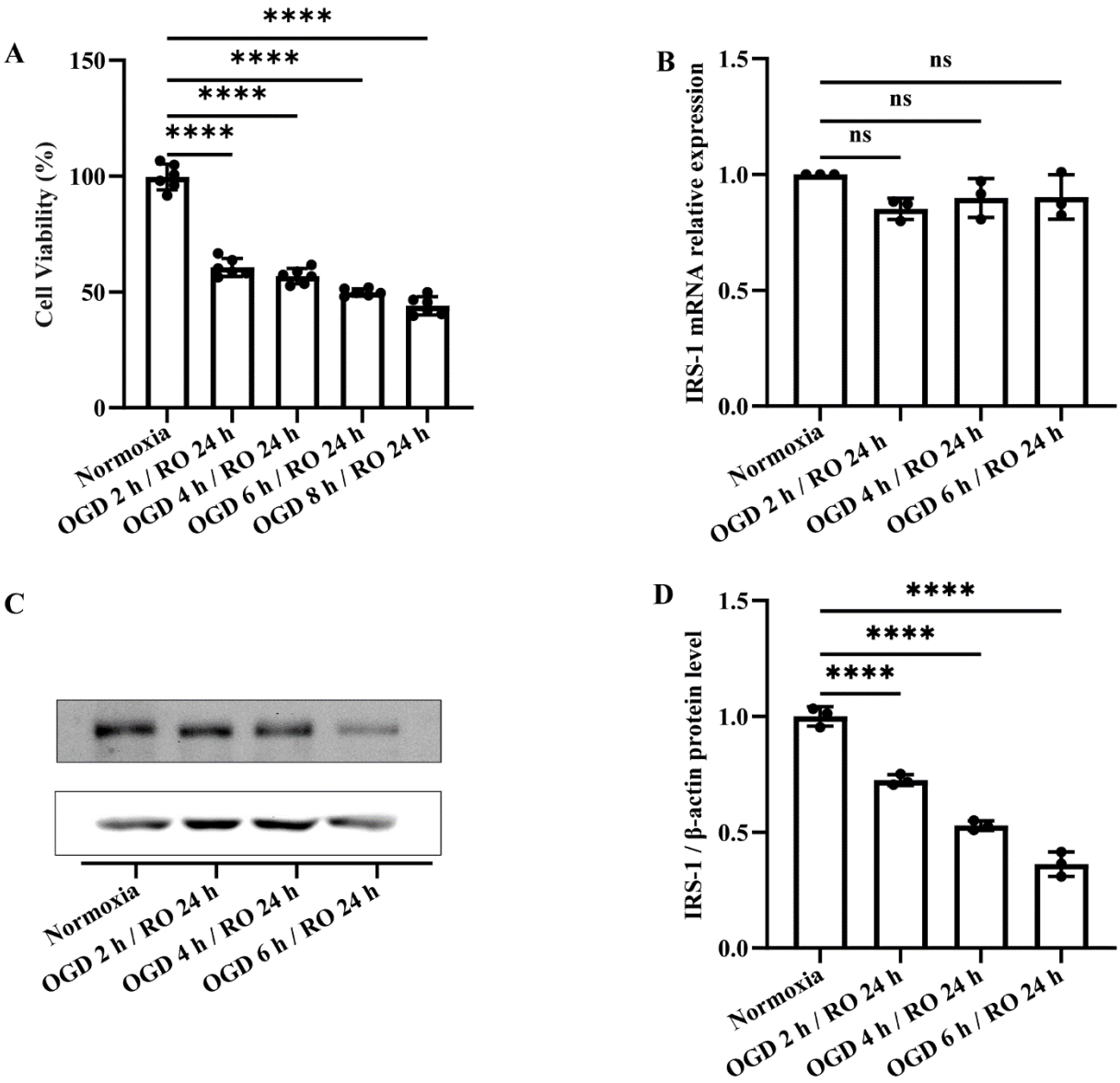

Figure 6. Establishment of OGD model and IRS-1 expression in primary neurons at different time points of OGD. A. MTT was used to test the cell viability of primary neurons exposed to 2 h, 4 h, 6 h, and 8 h of OGD followed by 24 h RO (n = 6). **B.** IRS-1 mRNA levels were measured by RT-qPCR in primary neurons subjected to OGD for 2 h, 4 h, and 6 h, followed by 24 h RO. **C, D.** Representative Western blot images showing IRS-1 protein expression in primary neurons subjected to OGD for 2 h, 4 h, and 6 h, followed by 24 h RO (n = 3). Data are presented as the mean ± standard deviation (SD). Statistical analysis was performed using one-way ANOVA. ****$p < 0.0001$, ns = not significant.

To validate these results at the cellular level, immunofluorescence staining was performed to examine IRS-1 expression in primary neurons following OGD treatment (**Figure 7A, B**). Neurons were identified using NeuN, a specific marker for mature neuronal nuclei, allowing precise assessment of IRS-1 expression within NeuN-positive cells. IRS-1 exhibited a cytoplasmic localization and was co-stained with NeuN. Quantitative analysis of IRS-1 fluorescence intensity was conducted using Image J software by measuring mean fluorescence signals within NeuN-

positive regions. In the normoxia group, IRS-1 expression was more abundant and diffusely distributed in the neuronal cytoplasm. In contrast, IRS-1 fluorescence intensity was significantly reduced in the OGD 4 h / RO 24 h group ($p < 0.05$), consistent with Western blot findings and further confirming the downregulation of IRS-1 protein expression under hypoxic stress (**Figure 7C, D**).

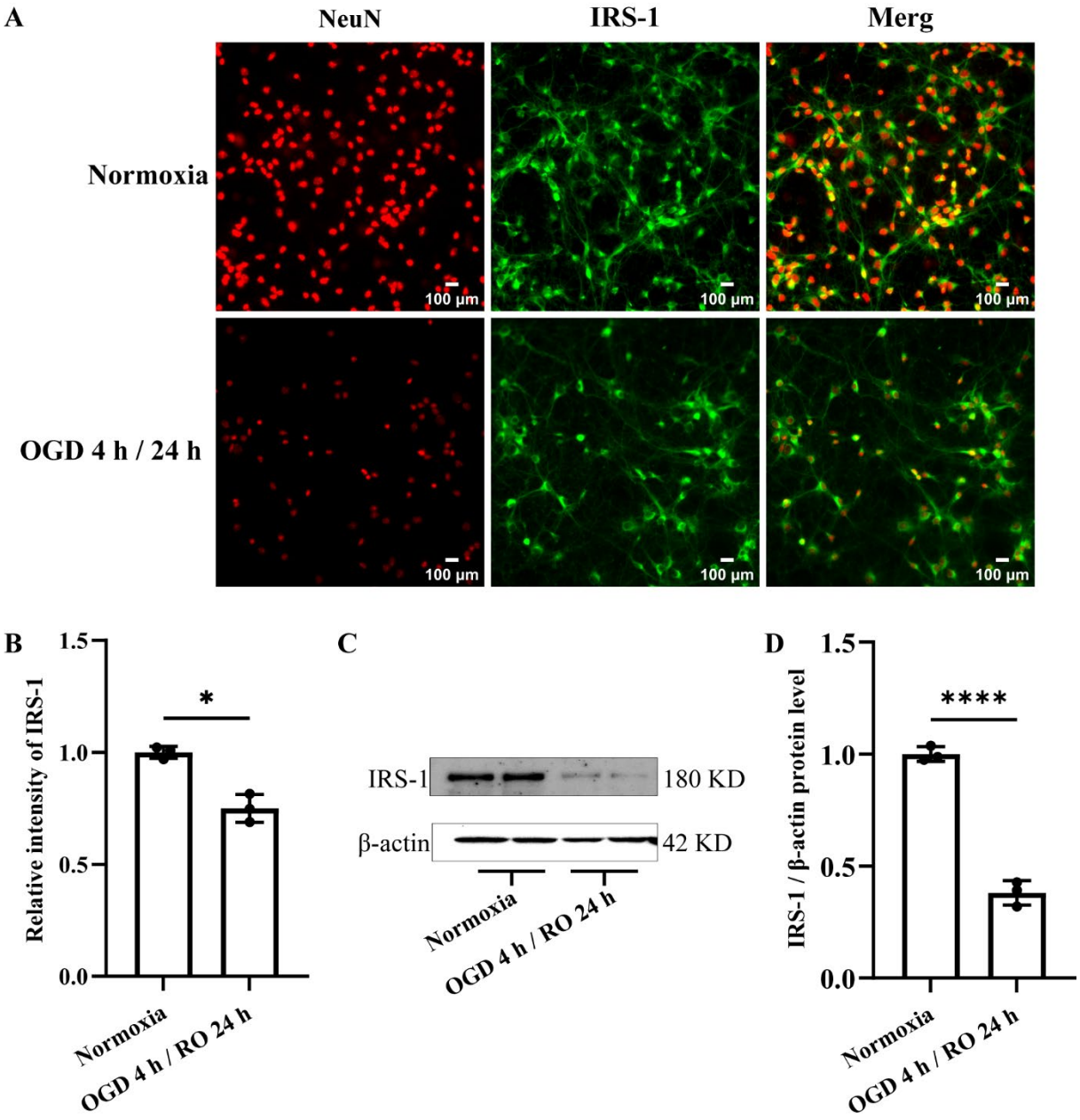

Figure 7 IRS-1 expression is decreased in primary neurons following OGD exposure. A, B. Immunofluorescence staining showing IRS-1 expression (green) in primary neuronal cytoplasm and NeuN expression (red) in neurons nuclei under normoxia and OGD 4 h / RO 24 h conditions. Scale bar = 100 μm. **C, D.** Representative Western blot images showing IRS-1 protein expression in primary neurons under Normoxia or after OGD 4 h / RO 24 h treatment. Data are presented as mean ± SD (n = 3). Statistical analysis was performed using t - test. *$p < 0.05$, ****$p<0.0001$.

3.3 OGD-induced reduction of IRS-1 in primary neurons is not mediated by proteasomal degradation

To investigate whether proteasomal degradation contributes to the OGD-induced reduction of IRS-1 in primary neurons, the proteasome inhibitor MG132 was applied at various concentrations (0.05 μM, 0.1 μM, 0.5 μM, 1 μM, and 5 μM). A normoxia group, maintained under standard culture conditions without OGD exposure, was used as the baseline control. Further analysis of MTT assay results demonstrated that low concentrations of MG132 (0.05 μM and 0.1 μM) significantly improved cell viability compared to the OGD / RO + DMSO group ($p < 0.0001$), whereas higher concentrations (0.5 μM, 1 μM, and 5 μM) failed to provide significant protective effects (**Figure 8A**). Based on these results, 0.05 μM and 0.1 μM MG132 were selected for subsequent experiments assessing IRS-1 protein expression

Western blot analysis revealed that despite the improved cell viability observed with 0.05 μM and 0.1 μM MG132 treatment, IRS-1 protein levels remained unchanged compared to the OGD / RO + DMSO group (ns, not significant; **Figure 8B, C**). In addition, MG132 treatment under normoxic conditions did not affect IRS-1 expression (**Figure 8D, E**).

These results suggest that proteasomal degradation is not a major contributor to the OGD-induced downregulation of IRS-1. The inability of MG132 to restore IRS-1 protein levels, despite enhancing neuronal viability, indicates that alternative mechanisms, such as autophagy-lysosomal degradation, may be responsible for IRS-1 reduction under hypoxic conditions.

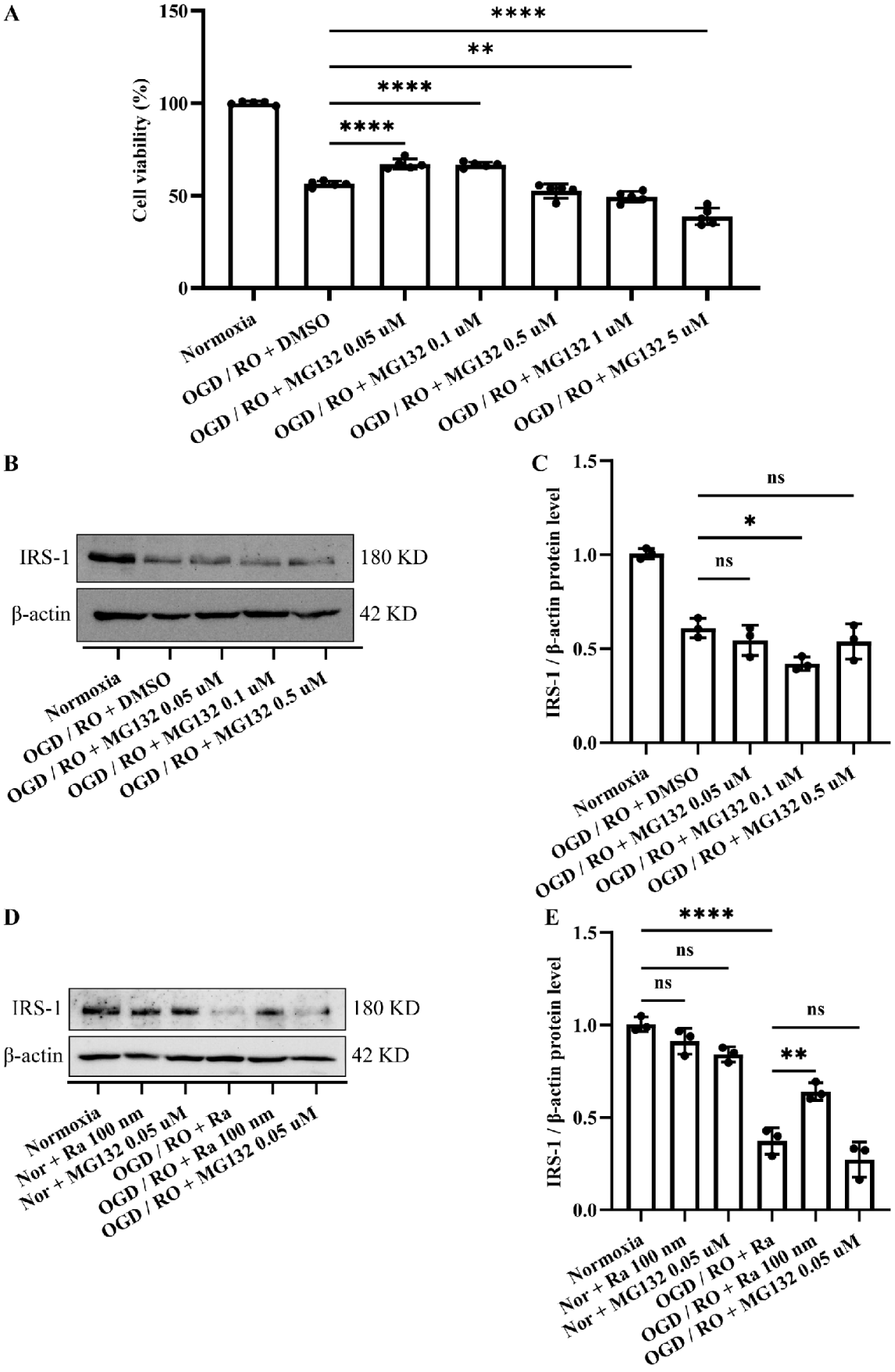

Figure 8 OGD-induced IRS-1 reduction in primary neurons is not mediated by proteasomal degradation. A. Cell viability assay showing the effect of OGD (4 h) followed by RO 24 h with or without

the proteasome inhibitor MG132 at different concentrations (0.05 μM, 0.1 μM, 0.5 μM, 1 μM and 5 μM) (n = 5). The two concentrations that significantly improved cell viability (0.05 μM and 0.1 μM) were selected for IRS-1 expression analysis. **B, C.** Representative Western blot images showing IRS-1 protein expression in primary neurons under Normoxia, OGD / RO + DMSO, and OGD / RO + MG132 (0.05 μM, 0.1 μM and 0.5 μM) conditions (n = 3). **D, E.** Under normoxic conditions, MG132 does not affect IRS-1 expression (n = 3). Data are presented as mean ± SD. Statistical analysis was performed one-way ANOVA. ****$p<0.0001$, ns = not significant.

3.4 OGD-induced reduction of IRS-1 in primary neurons is related to autophagy

To investigate whether or not autophagy contributes to the OGD-induced downregulation of IRS-1, primary neurons were treated with 3-methyladenine (3-MA), a widely used autophagy inhibitor, at various concentrations (0.1 mM, 0.5 mM, 1 mM, 1.5 mM, and 2.5 mM) under OGD conditions. A normoxia group, maintained under standard culture conditions without OGD exposure or drug treatment, served as the baseline control. Cell viability analysis revealed that 0.5 mM of 3-MA resulted in the highest neuronal viability among the treatment groups ($p < 0.0001$; **Figure 9A**). Western blot analysis further demonstrated that 3-MA treatment significantly increased IRS-1 protein expression compared to the OGD / RO + DMSO group, especially in the dose of 0.5mM 3-MA ($p < 0.001$; **Figure 9B, C**).

To determine whether the effect of 3-MA on IRS-1 expression was specific to hypoxic stress, we also applied 0.5 mM 3-MA under normoxic conditions. As shown in **Figure 9D, E**, 3-MA treatment had no significant impact on IRS-1 expression in normoxic neurons, indicating that the observed effect is specific to the OGD context.

To further explore the relationship between IRS-1 regulation and autophagy, we examined the protein levels of LC3 (microtubule-associated protein 1 light chain 3)-II/I, a commonly used marker of autophagic activity. LC3 plays a key role in autophagosome formation, and the conversion of LC3-I to its lipidated form LC3-II reflects autophagic flux (Runwal et al. 2019). Western blot analysis revealed that LC3-II levels were significantly reduced in 3-MA-treated neurons compared to the OGD control group ($p < 0.05$; **Figure 10A, B**), indicating that 3-MA effectively inhibited autophagy under OGD conditions.

Together, these findings suggest that OGD-induced downregulation of IRS-1 is mediated by autophagy. Inhibition of autophagy with 3-MA not only prevented the degradation of IRS-1 but also enhanced neuronal viability, highlighting a potential protective mechanism under hypoxic stress.

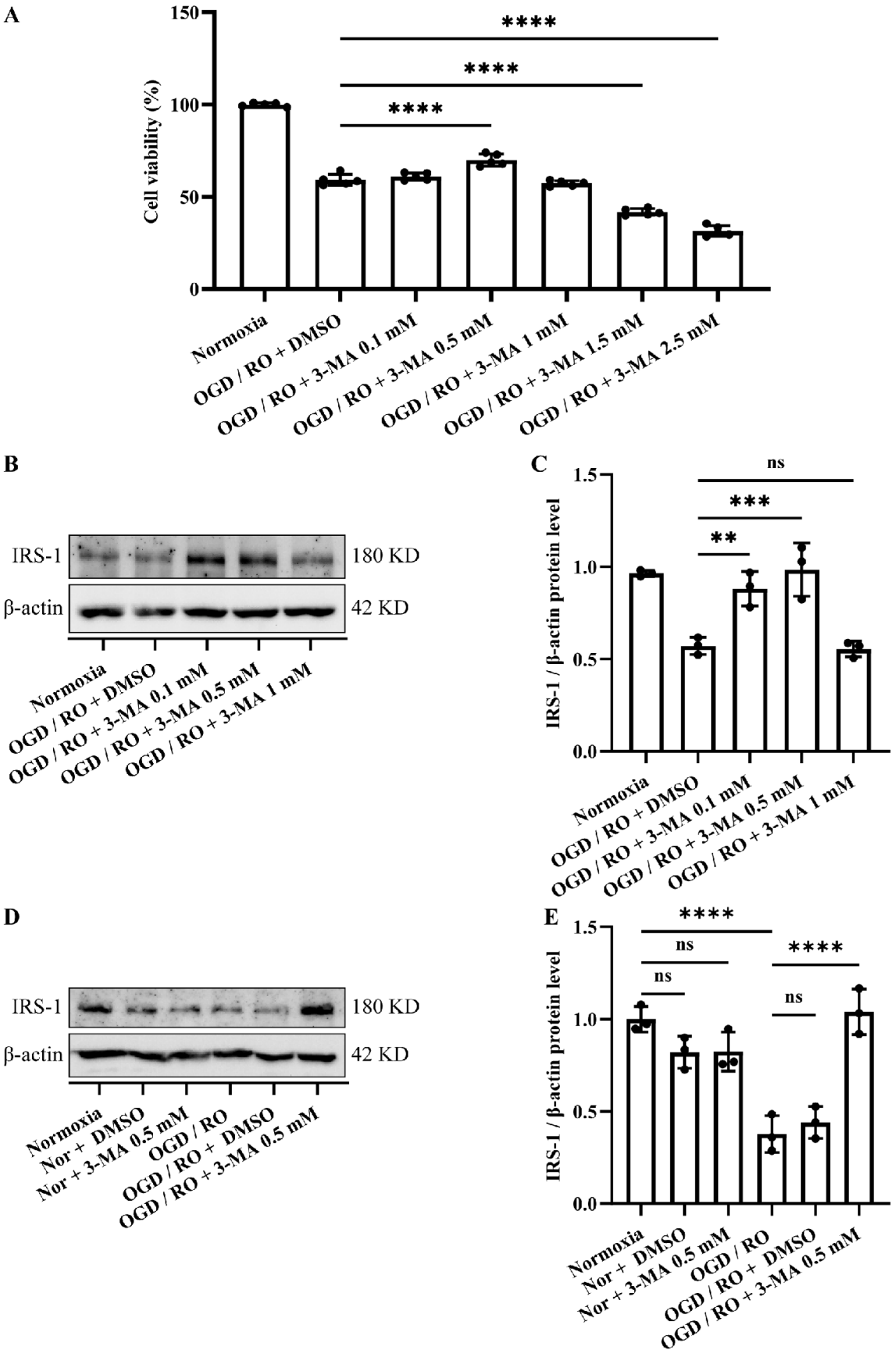

Figure 9. OGD-induced IRS-1 reduction in primary neurons is mediated by autophagy. A. Cell viability assay showing the effect of OGD (4 h) followed by RO 24 h with or without the autophagy inhibitor 3-MA at different concentrations (0.1 mM, 0.5 mM, 1 mM, 1.5 mM and 2.5 mM; n = 5). The

highest cell viability was observed at 0.5 mM 3-MA. **B, C.** Representative Western blot images showing IRS-1 protein expression in primary neurons under normoxia, OGD / RO + DMSO, and OGD / RO + 3-MA (0.1 mM, 0.5 mM and 1 mM) conditions (n = 3). **D, E.** under normoxic conditions, 3-MA does not affect IRS-1 expression. Data are presented as mean ± SD. Statistical analysis was performed using one-way ANOVA followed. *$p < 0.05$, **$p < 0.01$, ***$p < 0.001$, ****$p < 0.0001$, ns = not significant.

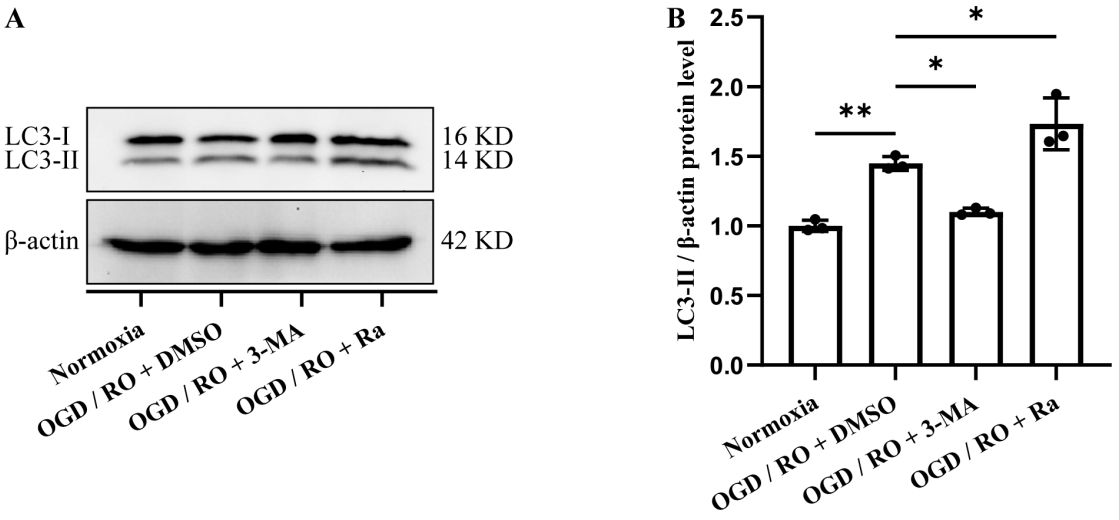

Figure 10. Effects of different treatments on LC3-II expression under OGD conditions. A. Representative Western blot images showing the levels of LC3-I and LC3-II in primary neurons under normoxia and OGD with different treatments: DMSO (vehicle control), 3-MA (autophagy inhibitor), and rapamycin (autophagy inducer). **B.** Quantification of LC3-II protein levels normalized to β-actin. Data are presented as mean ± SEM (n = 3). Statistical analysis was performed using one-way ANOVA followed. *$p < 0.05$, **$p < 0.01$.

3.5 Rapamycin can restore the IRS-1 degradation in primary neurons under OGD conditions

To investigate whether mTOR signaling is involved in OGD-induced IRS-1 downregulation, primary neurons were treated with rapamycin, an mTOR inhibitor and autophagy inducer, at various concentrations (50 nM, 100 nM, 150 nM, and 200 nM) under OGD conditions. A normoxia group, maintained under standard culture conditions without OGD or drug exposure, served as control. Cell viability analysis (**Figure 11A**) showed that rapamycin treatment did not improve neuronal survival under OGD conditions, as cell viability remained low across all tested concentrations. However, Western blot analysis **(Figure 11B, C**) revealed that treatment with 100 nM rapamycin partially restored IRS-1 protein expression compared to the OGD / RO + DMSO group.

To assess whether this effect was specific to hypoxic stress, 100 nM rapamycin was also applied under normoxic conditions. As shown in **Figure 8D, E**, rapamycin treatment did not significantly affect IRS-1 expression in normoxic neurons.

We further examined LC3-II/I protein levels to evaluate autophagic activity. As shown in **Figure 10 A, B**, rapamycin treatment increased LC3-II levels compared to the OGD control group ($p < 0.05$), indicating enhanced autophagy.

These results demonstrate that rapamycin partially restores IRS-1 expression under OGD conditions but does not enhance neuronal viability. Moreover, the increase in LC3-II suggests that rapamycin promotes autophagy while exerting differential effects on IRS-1 expression and cell survival.

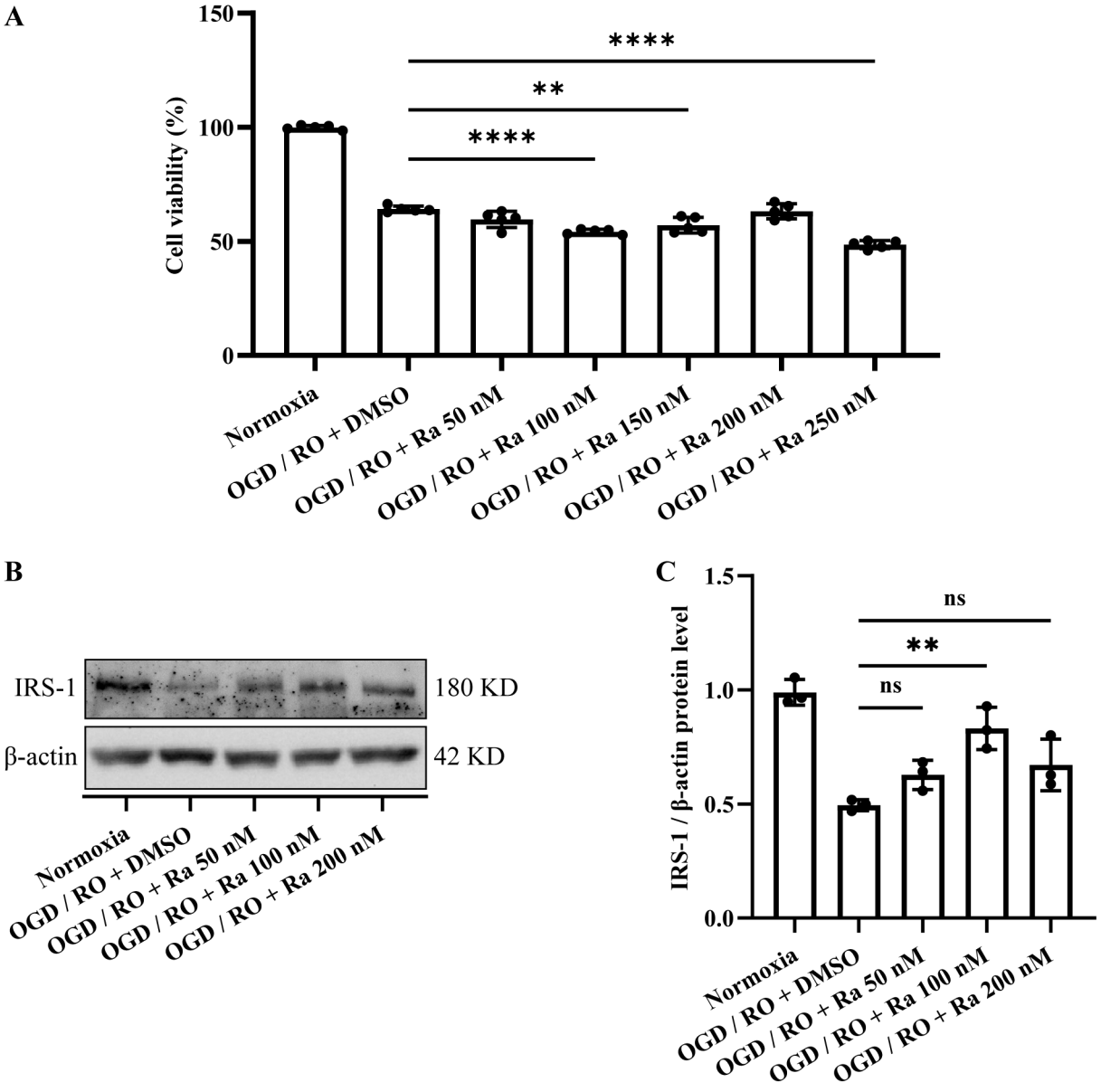

Figure 11. Rapamycin reverses OGD-induced IRS-1 degradation in primary neurons. A. Cell viability assay showing the effect of OGD (4 h) followed by RO 24 h with or without autophagy activator Rapamycin at different concentrations (50 nM, 100 nM, 150 nM, 200 nM， 250 nM) (n = 5). Rapamycin does not enhance cell viability. B, C. Representative Western blot images showing IRS-1 protein expression in primary neurons under Normoxia, OGD / RO + DMSO, and OGD / RO+ Rapamycin (50 nM, 100 nM, 200 nM) conditions (n = 3). Data are presented as mean ± SD. Statistical analysis was performed using one-way ANOVA followed **p < 0.01,****p < 0.0001. ns = not significant.

3.6 Effects of 3-MA and Rapamycin on IRS-1 Phosphorylation in primary neurons under OGD

To further investigate the regulatory mechanisms underlying IRS-1 degradation and its potential restoration by 3-MA and rapamycin, we examined two specific phosphorylation sites of IRS-1: Ser636/639 and Tyr608. Phosphorylation at Ser636/639 is associated with IRS-1 inhibition and degradation, often mediated by stress or mTOR activation, phosphorylation at Tyr608 is indicative of IRS-1 activation, particularly under hypoxic conditions, where it contributes to cellular stress adaptation and survival signaling (Martínez Báez et al. 2024). These two sites thus represent functionally opposing regulatory modifications and were selected to evaluate how autophagy inhibition or mTOR modulation affects IRS-1 signaling under OGD conditions.

Western blot analysis revealed that the level of p-IRS-1$^{Ser636/639}$ was significantly increased in the OGD / RO + DMSO group compared to the normoxia group ($p < 0.0001$), indicating enhanced inhibitory phosphorylation under hypoxic stress. In contrast, treatment with either 3-MA or rapamycin significantly reduced p-IRS-1$^{Ser636/639}$ expression (**Figure 12A, B**), suggesting a reversal of this inhibitory modification.

Regarding p-IRS-1^{Tyr608}, the protein signal was barely detectable under both normoxia and OGD conditions, likely due to low basal phosphorylation at this site in the absence of stimulation. However, treatment with either 3-MA or rapamycin markedly increased p-IRS-1^{Tyr608} levels ($p < 0.0001$; **Figure 12C, D**), indicating enhanced IRS-1 activation in response to these interventions. Although the signal intensity was low, Western blotting still allowed the detection of significant differences between groups, suggesting the method was sufficiently sensitive for relative comparison in this context.

Collectively, these findings suggest that autophagy inhibition prevents the OGD-induced increase in inhibitory IRS-1 phosphorylation (Ser636/639) while promoting its activating phosphorylation (Tyr608). Similarly, rapamycin—through mTOR inhibition—also decreases p-IRS-1$^{Ser636/639}$ and enhances p-IRS-1^{Tyr608}, indicating modulation of IRS-1 signaling through distinct mechanisms.

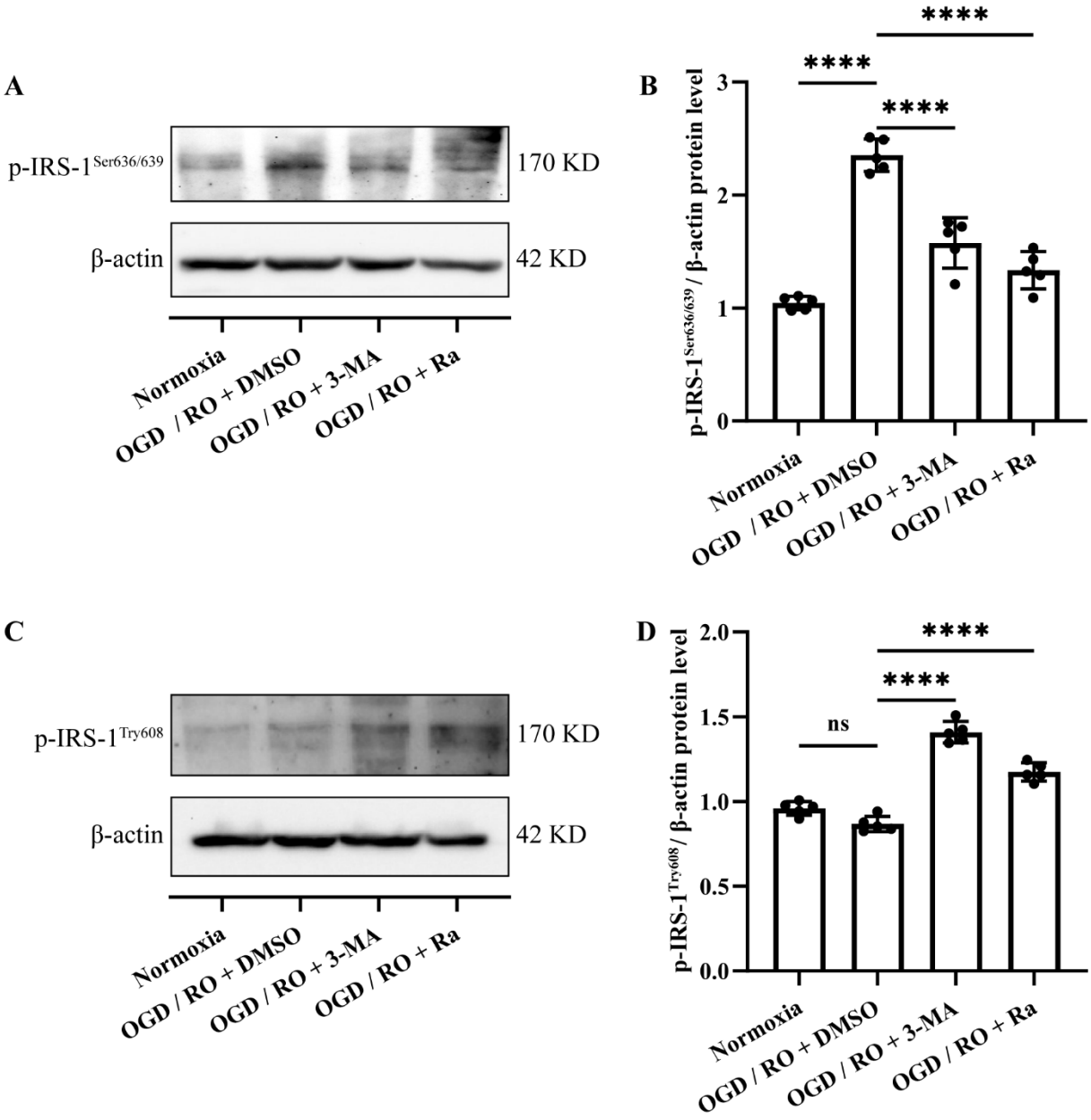

Figure 12 The effect of autophagy inhibition (3-MA) and Rapamycin on IRS-1 phosphorylation in primary neurons under OGD conditions. A, B. Representative Western blot images showing p-IRS-1$^{Ser636/639}$ protein expression in primary neurons under Normoxia, OGD / RO + DMSO, OGD / RO + 3-MA and OGD / RO + Rapa (n = 5). **C, D.** Representative Western blot images showing p-IRS-1^{Tyr608} protein expression in primary neurons under Normoxia, OGD / RO + DMSO, OGD / RO + 3-MA and OGD / RO + Rapa (n = 5). Data are presented as mean ± SD. Statistical analysis was performed using one-way ANOVA followed $^{****}p < 0.0001$.

4 DISCUSSION

Ischemic cerebrovascular disease is a leading global health concern, with high disability and mortality rates imposing significant burdens on families and society. Despite advances in understanding its pathophysiology, the mechanisms of injury and repair remain key research priorities. Stroke initiates a cascade of pathological events affecting both neurons and endothelial cells. Neuronal damage results from energy depletion, excitotoxicity, oxidative stress, and inflammation, ultimately leading to cell death (Qin et al. 2022; Zhao et al. 2022). Meanwhile, ischemia disrupts vascular integrity, causing blood-brain barrier breakdown and inflammation, while also triggering vascular repair and angiogenesis (Moon et al. 2021). Understanding these processes is crucial for developing therapies that minimize neuronal and vascular injury while promoting recovery.

IRS-1 is widely expressed in neurons and endothelial cells (Gual, Le Marchand-Brustel, and Tanti 2005; Huang, Lee, and Hsu 2010). It is hypothesized that IRS-1 may exert neuroprotective effects by inhibiting neuronal apoptosis. Additionally, IRS-1 is known to protect vascular endothelial cells. For instance, IRS-1 has been reported to exert protective effects against ox-LDL-induced atherosclerosis injury by inhibiting ER stress/oxidative stress-mediated apoptosis and activating the Akt/FoxO1 signaling pathway (Liu et al. 2020). In Diabetes and IR, IRS-1 enhances the expression of vascular endothelial growth factor (VEGF), promotes angiogenesis, improves endothelial repair, and accelerates wound healing (Katagiri et al. 2016).

However, there is also evidence that IRS-1 may have adverse effects under certain pathological conditions. For example, studies on neonatal rats subjected to hypoxic-ischemic conditions have shown that overexpression of IRS-1 in endothelial cells using transgenic models exacerbates vascular barrier disruption and increases brain tissue damage. Conversely, overexpression of IRS-1 in neurons under the same conditions has been found to reduce neuronal apoptosis, enhance cell survival, and mitigate brain injury (Tu et al. 2021). The precise mechanisms underlying these effects remain unclear. The aim of this study is to investigate the changes in IRS-1 expression following hypoxia and to elucidate the specific mechanisms by which IRS-1 exerts neuroprotective effects under hypoxia conditions.

4.1 Identification of primary neurons, and establishment of OGD model in vitro

In this study, the successful isolation and identification of primary neurons were critical steps in ensuring the reliability and relevance of the experimental model. Primary neurons were isolated from embryonic mouse brains, a commonly used model for neuronal studies due to the purity and consistency of the cultures (Kaech and Banker 2006). After isolation, the neurons were identified by immunofluorescence staining using neuron-specific marker NeuN, which is exclusively expressed in neuronal cells (**Figure 5**) (Zhang et al. 2021). To simulate ischemic-like conditions in vitro, we successfully established an OGD model, which mimics the hypoxic and nutrient-deprived environment experienced by neurons during ischemic events such as stroke (Ryou and Mallet 2018). The OGD model was created by incubating the primary neurons in a glucose-free medium within a hypoxic chamber at 1.5% oxygen for a defined period. The duration of OGD was optimized to induce measurable cellular and molecular changes while maintaining cell viability for downstream analyses (Kuang et al. 2020). This model has been widely used to investigate the mechanisms of neuronal injury, cell survival, and neuroprotection under ischemic conditions.

After constructing the OGD model, the cell viability of primary neurons was assessed to validate the extent of injury and ensure reproducibility of the experimental conditions. Cell viability was measured using the MTT assay, a widely used method for evaluating mitochondrial metabolic activity as an indicator of cell health. In this experiment, neurons exposed to OGD showed a significant reduction in cell viability compared to normoxic controls, with viability decreasing by approximately 50% after 4 hours of hypoxia (**Figure 6A**). This decline aligns with the expected cellular injury caused by hypoxic conditions (Li et al. 2017).

Overall, the combination of primary neuronal cultures and the OGD model provides a robust in vitro platform to study the molecular mechanisms underlying neuronal injury and repair under hypoxic conditions (Ryou and Mallet 2018). This approach allows for precise control of experimental variables, enabling reproducible investigations into neuroprotective strategies and therapeutic interventions for ischemic brain injury.

4.2 IRS-1 is downregulated in primary neurons exposed to OGD

It is well established that insulin or insulin-like growth factor 1 (IGF-1) stimulation can activate IRS-1, mediating downstream signaling pathways. However, prolonged insulin exposure has been shown to reduce IRS-1 expression, leading to insulin desensitization and insulin resistance (Copps and White 2012). IRS-1 is widely expressed in central neurons and endothelial cells,

and previous studies have demonstrated that chronic insulin stimulation decreases IRS-1 expression in neurons (Lee et al. 2009; Mayer and Belsham 2010). Existing studies indicate that under oxidative stress, IRS-1 expression is reduced in multiple cell types, including mouse embryonic fibroblasts (MEFs) (Kang, Brown, and Chung 2007). Nevertheless, research on the regulation of IRS-1 under hypoxic conditions is limited. Our study investigated IRS-1 expression in primary neurons subjected to OGD, an in vitro model mimicking ischemic stroke conditions. Using qPCR analysis, we found that IRS-1 mRNA levels did not exhibit significant changes under hypoxia (**Figure 6B**). Interestingly, however, Western blot analysis revealed a significant reduction in IRS-1 protein levels (Figure 4), suggesting a post-transcriptional regulatory mechanism. These findings indicate that hypoxia may promote IRS-1 degradation rather than suppress its gene transcription, possibly through proteasomal degradation pathways or autophagy-associated mechanisms.

4.3 Possible mechanisms of IRS-1 downregulation under hypoxia conditions

IRS-1 is a pivotal adaptor protein in insulin signaling, and its degradation is intricately regulated by various cellular mechanisms, including ubiquitination, autophagy, and the mTOR/S6K1 pathway according to different condition (Mayer and Belsham 2010).

4.3.1 Ubiquitin-proteasome system is not the main pathway mediating IRS-1 degradation under hypoxic conditions

Under the intervention of insulin, IRS-1 undergoes ubiquitination, marking it for proteasomal degradation. The E3 ubiquitin ligase complex SCF^β-TRCP plays a significant role in this process. Specifically, mTORC1 phosphorylates IRS-1 at Serine 422, creating a binding site for β-TRCP (Yoneyama et al. 2018). This interaction leads to IRS-1 ubiquitination and subsequent degradation, serving as a feedback mechanism to modulate insulin signaling. Insulin resistance mechanisms often involve phosphorylation of IRS-1 at specific serine residues (e.g., Ser307, Ser636/639), promoting its dissociation from the insulin receptor and targeting it for ubiquitination (Copps and White 2012). However, our results indicate that the proteasome inhibitor MG132 did not restore IRS-1 expression under hypoxic conditions (**Figure 8**), suggesting that ubiquitination-mediated proteasomal degradation is not the primary mechanism driving IRS-1 downregulation in hypoxia, which indicated the same result of the previous research (Kang, Brown, and Chung 2007). And the IRS-1 degradation induced by prolonged insulin intervention and hypoxia may involve different mechanisms. Our findings suggest that under hypoxia, the

proteasomal pathway is not responsible for IRS-1 degradation, indicating an alternative regulatory mechanism, likely involving autophagy or mTOR signaling pathways.

4.3.2 Autophagy inhibition reverses IRS-1 degradation under hypoxia by modulating IRS-1 phosphorylation

4.3.2.1 Autophagy inhibition reverses IRS-1 degradation under hypoxia

Previous studies have explored the mechanisms underlying IRS-1 degradation in hypoxic conditions. Kang et al. demonstrated that transient hypoxia (1% oxygen) induces caspase-mediated cleavage of IRS-1, suggesting that reduced Akt signaling may contribute to IRS-1 degradation, as Akt normally inhibits caspase activation. Additionally, IRS-1 loss was prevented by protein tyrosine phosphatase (PTP) inhibitors, indicating that hypoxia-induced dephosphorylation plays a role in its degradation (Kang, Brown, and Chung 2007). While caspase activation and dephosphorylation are implicated in IRS-1 degradation, our findings suggest that autophagy is also a key contributor.

We observed that under hypoxic conditions, primary neurons exhibited increased LC3-II levels, a marker of autophagosome formation, alongside a reduction in IRS-1 expression (**Figure 10**). Notably, treatment with the autophagy inhibitor 3-methyladenine (3-MA) significantly restored IRS-1 expression (**Figure 9)**, suggesting that IRS-1 is primarily degraded through the autophagic-lysosomal pathway rather than the ubiquitin-proteasome system. Given that autophagy plays a critical role in cellular adaptation to hypoxia by degrading damaged proteins and organelles to maintain energy homeostasis (Dai et al. 2024), it is possible that IRS-1 is selectively targeted for degradation under these conditions, similar to what has been observed in metabolic stress models where autophagy impairs insulin signaling by degrading IRS-1 (Frendo-Cumbo et al. 2019; Igawa et al. 2019).

4.3.2.2 Autophagy inhibition mediated IRS-1 degradation through IRS-1 phosphorylation modulation

Autophagy plays a dual role in neuronal health: while basal autophagy is essential for cellular homeostasis by removing damaged organelles and misfolded proteins, excessive autophagy can lead to autophagic stress, exacerbating neuronal injury and accelerating cell death (Cherra and Chu 2008). Our findings suggest that autophagy inhibition under hypoxia may provide neuroprotection, not only by preventing IRS-1 degradation but also by modulating its phosphorylation state.

Phosphorylation of IRS-1 at tyrosine residues is crucial for activating downstream signaling pathways, particularly the PI3K/Akt pathway, which promotes neuronal survival and growth. Conversely, serine phosphorylation often acts as a negative regulatory mechanism, inhibiting insulin signaling and contributing to cellular stress responses (Zheng and Wang 2021). We observed that 3-MA treatment under hypoxia not only restored IRS-1 levels but also enhanced p-IRS-1Tyr608 while reducing p-IRS-1Ser636/639 (**Figure 12**), suggesting that autophagy inhibition may relieve IRS-1 suppression and restore its signaling function.

Previous studies have shown that reduced IRS-1 serine phosphorylation can lead to an increase in tyrosine phosphorylation, subsequently activating the PI3K/Akt pathway(Copps and White 2012). This mechanism may explain how autophagy inhibition confers cell viability in hypoxic conditions by stabilizing IRS-1 and promoting its tyrosine phosphorylation, it enhances downstream survival signaling.

4.3.3 Rapamycin Reverses IRS-1 Degradation Under Hypoxic Conditions via mTOR/S6K1 Signaling

4.3.3.1 Rapamycin Restores IRS-1 Expression Under Hypoxia

Our study demonstrates that rapamycin, an mTOR inhibitor, effectively prevents the degradation of IRS-1 in primary neuronal cells under hypoxic conditions (**Figure 11**). Hypoxia is known to induce metabolic stress and disrupt insulin signaling, partly through the degradation of IRS-1, a key mediator of insulin receptor function(Kang, Brown, and Chung 2007). However, treatment with rapamycin significantly restores IRS-1 protein levels, suggesting that mTOR-dependent mechanisms contribute to IRS-1 downregulation under hypoxic conditions. Given that rapamycin is a well-known autophagy activator, its ability to preserve IRS-1 expression under hypoxia presents an apparent contradiction -one would expect that increased autophagy would enhance IRS-1 degradation. However, our results suggest that the restoration of IRS-1 by rapamycin occurs via an alternative mechanism that is distinct from its autophagy-promoting function.

To investigate the mechanism by which rapamycin preserves IRS-1 expression, we examined IRS-1 phosphorylation patterns under hypoxia. Our findings indicate that: Hypoxia increases p-IRS-1Ser636/639 (**Figure 12**), a modification that is typically associated with IRS-1 degradation and impaired insulin signaling. Rapamycin treatment significantly reduces p-IRS-1Ser636/639 (**Figure 12**), suggesting that the mTOR signaling pathway is involved in IRS-1

regulation under hypoxia. Additionally, rapamycin enhances p-IRS-1Tyr608, a marker of IRS-1 activation, further supporting the idea that rapamycin preserves IRS-1 function.
These findings align with previous studies demonstrating that IRS-1 degradation can be mediated by the mTOR-S6K1 signaling pathway, which negatively regulates IRS-1 expression via phosphorylation at serine residues such as Ser636/639 or Ser1101 (Mayer and Belsham 2010; Tremblay et al. 2007; Tzatsos and Kandror 2006).

4.3.3.2 mTOR/S6K1 Pathway and IRS-1 Degradation

mTOR is a serine/threonine kinase that plays a pivotal role in regulating cellular metabolism, growth, proliferation, and autophagy. It integrates various signals, including nutrient availability, growth factors, and energy status, to modulate cellular processes. mTOR exists in two functionally distinct complexes: mTOR Complex 1 (mTORC1): This complex is primarily involved in protein synthesis, lipid metabolism, and autophagy suppression. It is activated by insulin, amino acids, and growth factors and can phosphorylate downstream targets such as S6 kinase 1 (S6K1) and 4E-binding protein 1 (4E-BP1), which promote mRNA translation and protein synthesis (Laplante and Sabatini 2012). Importantly, mTORC1 also negatively regulates insulin signaling by promoting IRS-1 degradation via S6K1 activation. mTOR Complex 2 (mTORC2): This complex is primarily involved in cytoskeletal organization, cell survival, and Akt signaling. Unlike mTORC1, mTORC2 does not directly regulate protein synthesis but plays a role in insulin signaling by phosphorylating Akt at Ser473, enhancing its activation (Sarbassov et al. 2005).
Under normal physiological conditions, mTORC1-S6K1 signaling negatively regulates IRS-1 function through phosphorylation at specific serine residues, such as Ser636. This process follows a well-established feedback loop: Insulin stimulation activates the PI3K/Akt pathway, leading to mTORC1 activation. Activated mTORC1 phosphorylates and activates S6K1, which in turn phosphorylates IRS-1 at Ser636 (or equivalent serine residues such as Ser307 and Ser1101 in different cell types) (Harrington et al. 2004; Tremblay et al. 2007). Serine phosphorylation of IRS-1 marks it for degradation, leading to decreased IRS-1 levels and a reduction in insulin receptor signaling (Mayer and Belsham 2010).This creates a negative feedback loop, where persistent mTORC1 activation leads to insulin resistance by reducing IRS-1 stability (Tzatsos and Kandror 2006).
Given that mTORC1 activation promotes IRS-1 degradation, it follows that inhibiting mTORC1 could prevent IRS-1 degradation and restore insulin sensitivity. Rapamycin, a selective mTORC1 inhibitor, suppresses S6K1 activation, preventing it from phosphorylating IRS-

1 at Ser636. This reduces IRS-1 degradation and stabilizes its expression, thereby enhancing insulin receptor signaling. Several studies have demonstrated that inhibiting mTORC1 improves insulin sensitivity by reducing IRS-1 serine phosphorylation and preserving IRS-1 function (Copps and White 2012; Harrington et al. 2004; Tremblay et al. 2007).

4.4 Summary

Stroke remains a major global health concern due to its high incidence, disability rate, and recurrence. Among the pathological changes following stroke, neuronal death plays a central role in the progression of neurological deficits. Alleviating neuronal injury and rescuing the ischemic penumbra are key objectives in stroke research, with an urgent need for effective therapeutic strategies.

This study investigates the protective role of IRS-1 in primary neurons under oxygen-glucose deprivation, an in vitro model that mimics ischemic stroke. Under hypoxic conditions, IRS-1 protein expression is significantly reduced, while mRNA levels remain unchanged, suggesting post-transcriptional regulation, potentially through protein degradation or modification.

To explore the mechanisms underlying IRS-1 downregulation, neuronal cultures were treated with MG132 (a proteasome inhibitor), 3-MA (an autophagy inhibitor), and rapamycin (an autophagy activator). MG132 treatment did not restore IRS-1 levels, indicating that proteasomal degradation is not the primary pathway. However, both 3-MA and rapamycin effectively increased IRS-1 protein expression, implicating autophagy as a key regulatory mechanism.

Further analysis of LC3-II expression confirmed autophagy involvement. Phosphorylation levels of IRS-1 at Tyr608 and Ser636/639 were examined, revealing that 3-MA increased p-IRS-1Tyr608 and decreased p-IRS-1$^{Ser636/639}$, suggesting that the restoration of IRS-1 is related to phosphorylation status. Rapamycin likely acts through the mTOR/S6K1 pathway to modulate p-IRS-1$^{Ser636/639}$, thereby reducing IRS-1 degradation.

These findings indicate that IRS-1 plays a potential neuroprotective role under hypoxic conditions by resisting autophagy-related degradation. The results provide mechanistic insights into IRS-1 regulation in ischemic conditions and support its potential as a therapeutic target for stroke intervention.

4.5 Outlook

Building upon the findings of this study, several future experiment can be considered to deepen our understanding of IRS-1 regulation under hypoxic conditions. First, although MG132 treatment suggests a role for the UPS in IRS-1 degradation, future studies could perform immunoprecipitation (IP) assays to directly investigate the interaction between IRS-1 and ubiquitin. This would help clarify the contribution of ubiquitination to IRS-1 stability. Second, while rapamycin treatment indicated possible involvement of the mTOR/S6K1 pathway, direct assessment of mTOR/S6K1 expression and phosphorylation levels under hypoxia would strengthen the mechanistic insight. Third, the potential contribution of the lysosomal pathway to IRS-1 degradation warrants further exploration, for instance by using lysosomal inhibitors such as chloroquine, along with additional autophagy-related markers (e.g., p62, ATG proteins) to delineate specific autophagy stages involved. Moreover, expanding the phosphorylation profiling of IRS-1 beyond Ser636/639 and Tyr608 to include other regulatory Ser and Tyr residues may provide a more comprehensive understanding of its post-translational modification landscape. Lastly, functional studies involving IRS-1 overexpression or knockdown in primary neurons would be essential to directly evaluate its neuroprotective potential under hypoxic stress.

5 ABSTRACT

Stroke is a major cause of death and disability worldwide, with neuronal death as a key factor. IRS-1, a core insulin signaling protein, may support neuronal survival under hypoxic conditions. In this study, primary cortical neurons were subjected to oxygen-glucose deprivation (OGD) followed by 24 hours of reoxygenation to mimic ischemic injury. Cell viability was significantly reduced, with approximately 50% neuronal death observed under these conditions. Interestingly, while IRS-1 mRNA levels remained relatively stable, a marked and time-dependent decrease in IRS-1 protein was detected, suggesting post-transcriptional regulation. Immunofluorescence confirmed the loss of IRS-1 expression in neurons after OGD. To explore the mechanism of IRS-1 degradation, we applied MG132 (a proteasome inhibitor), 3-MA (an autophagy inhibitor), and Rapamycin (an autophagy activator via mTOR inhibition). While MG132 improved cell viability, it did not restore IRS-1 levels, indicating that proteasomal degradation was not the dominant pathway. In contrast, inhibition of autophagy via 3-MA significantly increased IRS-1 expression and decreased LC3-II levels, a marker of autophagic flux. Rapamycin, surprisingly, also partially restored IRS-1 protein levels despite promoting autophagy, suggesting a modulatory effect through the mTOR/S6K1 pathway. Furthermore, Western blot analysis revealed a substantial increase in Ser636/639 phosphorylation of IRS-1 under OGD, a modification known to target IRS-1 for degradation. Both 3-MA and Rapamycin significantly reduced this phosphorylation, while simultaneously enhancing Tyr608 phosphorylation, a site associated with IRS-1 activation. These findings suggest that under ischemic stress, IRS-1 undergoes degradation primarily through autophagy linked with stress-induced phosphorylation at Ser636/639. Modulation of autophagy pathways or phosphorylation status could thus be a promising strategy to preserve IRS-1 function and support neuronal survival. Altogether, this study highlights IRS-1 as a potential neuroprotective factor and therapeutic target for the treatment of ischemic stroke.

6 ZUSAMMENFASSUNG

Schlaganfall ist weltweit eine der häufigsten Todesursachen und Hauptursache für Behinderungen. Der neuronale Zelltod spielt eine Schlüsselrolle. IRS-1, ein zentrales Protein der Insulin-Signalkaskade, könnte unter Hypoxie das neuronale Überleben fördern. In dieser Studie wurden primäre kortikale Neurone einem Sauerstoff- und Glukoseentzug (OGD) unterzogen, gefolgt von 24 Stunden Reoxygenierung, um eine ischämische Schädigung zu modellieren. Die Zellvitalität war unter diesen Bedingungen mit ca. 50 % deutlich reduziert. Interessanterweise blieben die mRNA-Spiegel von IRS-1 relativ stabil, jedoch zeigte sich ein ausgeprägter, zeitabhängiger Rückgang des IRS-1-Proteins, was auf eine posttranskriptionelle Regulation hinweist. Die Immunfluoreszenz bestätigte den Verlust der IRS-1-Expression in Neuronen nach OGD. Zur Untersuchung des Abbaumechanismus von IRS-1 wurden MG132 (ein Proteasominhibitor), 3-MA (ein Autophagieinhibitor) und Rapamycin (ein Autophagieaktivator über mTOR-Hemmung) eingesetzt. Während MG132 die Zellvitalität verbesserte, wurde der IRS-1-Spiegel nicht wiederhergestellt. Dies deutet darauf hin, dass der proteasomale Abbau nicht der dominierende Weg ist. Im Gegensatz dazu führte die Hemmung der Autophagie durch 3-MA zu einer signifikanten Erhöhung der IRS-1-Expression und zu einer Reduktion von LC3-II, einem Marker für den Autophagiefluss. Überraschenderweise stellte auch Rapamycin trotz Förderung der Autophagie den IRS-1-Proteinspiegel teilweise wieder her, was auf einen modulierenden Effekt über den mTOR/S6K1-Signalweg hindeutet. Die Western-Blot-Analysen zeigten zudem unter OGD-Bedingungen eine deutliche Zunahme der Phosphorylierung von IRS-1 an Ser636/639, einer Modifikation, die als Signal für den Proteinabbau bekannt ist. Sowohl 3-MA als auch Rapamycin reduzierten diese Phosphorylierung signifikant und erhöhten gleichzeitig die Tyr608-Phosphorylierung, eine Modifikation, die mit der Aktivierung von IRS-1 assoziiert ist. Diese Ergebnisse deuten darauf hin, dass IRS-1 unter hypoxischem Stress vorwiegend durch autophagischen Abbau infolge stressinduzierter Ser636/639-Phosphorylierung degradiert wird. Eine Modulation der Autophagiepfade oder des Phosphorylierungsstatus könnte daher eine vielversprechende Strategie darstellen, um die Funktion von IRS-1 zu erhalten und das Überleben von Neuronen zu fördern. Insgesamt identifiziert diese Studie IRS-1 als potenziellen neuroprotektiven Faktor und therapeutisches Ziel zur Behandlung des ischämischen Schlaganfalls.

7 ABBREVIATION

Akt	Protein Kinase B
AMPA	α-Amino-3-hydroxy-5-methyl-4-isoxazolepropionic acid
ANOVA	Analysis of Variance
APS	Ammonium Persulfate
ATP	Adenosine Triphosphate
ATG	Autophagy-related Gene
BBB	Blood-Brain Barrier
BSA	Bovine Serum Albumin
BSS	Balanced Salt Solution
BSS0	Balanced Salt Solution (glucose-free)
CBF	Cerebral Blood Flow
CNS	Central Nervous System
CRL7	Cullin-RING E3 Ubiquitin Ligase 7
CUL3	Cullin 3
CUL7	Cullin 7
cRPM	Centrifuge Revolutions Per Minute
DAPI	4′,6-diamidino-2-phenylindole
DMEM	Dulbecco’s Modified Eagle Medium
DMSO	Dimethyl Sulfoxide
DNAse I	Deoxyribonuclease I
DPBS	Dulbecco's Phosphate Buffered Saline
EAA	Excitatory Amino Acids
ECL	Enhanced Chemiluminescence
eNOS	Endothelial Nitric Oxide Synthase
ERK	Extracellular signal-Regulated Kinase
FBS	Fetal Bovine Serum
GFP	Green Fluorescent Protein
GLUT4	Glucose Transporter Type 4
GSK-3β	Glycogen Synthase Kinase 3 Beta
HRP	Horseradish Peroxidase
ICH	Intracerebral Hemorrhage

IGF-1	Insulin-like Growth Factor 1
IL-1	Interleukin-1
IR	Insulin Receptor
IRS	Insulin Receptor Substrate
IRS-1	Insulin Receptor Substrate 1
IKKβ	IκB Kinase β
JNK	c-Jun N-terminal Kinase
KLHL9	Kelch-like protein 9
KLHL13	Kelch-like protein 13
3-MA	3-Methyladenine
MAPK	Mitogen-Activated Protein Kinase
MEF	Mouse Embryonic Fibroblast
MEK	MAPK/ERK Kinase
MG132	Proteasome Inhibitor
min	Minute
mM / μM	Millimolar / Micromolar
mRNA	Messenger RNA
mTOR	Mechanistic Target of Rapamycin
mTORC1 / mTORC2	mTOR Complex 1 / 2
MTT	3-(4,5-dimethylthiazol-2-yl)-2,5-diphenyl tetrazolium bromide
NeuN	Neuronal Nuclei Marker
nm	Nanometer
NMDA	N-Methyl-D-Aspartate
NO	Nitric Oxide
OGD	Oxygen-Glucose Deprivation
PAGE	Polyacrylamide Gel Electrophoresis
PARP	Poly (ADP-ribose) Polymerase
RT-qPCR	Quantitative Real-Time PCR
PDK1	3-Phosphoinositide-dependent protein kinase-1
PFA	Paraformaldehyde
PH	Pleckstrin Homology (domain)
PI3K	Phosphoinositide 3-Kinase
PIP2 / PIP3	Phosphatidylinositol 4,5-bisphosphate / 3,4,5-trisphosphate

PFO	Patent Foramen Ovale
PTB	Phosphotyrosine Binding domain
PTP	Protein Tyrosine Phosphatase
PVDF	Polyvinylidene Difluoride
qRT-PCR	Quantitative Reverse Transcription PCR
Rapa	Rapamycin
RIPA	Radioimmunoprecipitation Assay
RO	Reoxygenation
ROS	Reactive Oxygen Species
RT	Room Temperature
rt-PA	Recombinant Tissue Plasminogen Activator
SAH	Subarachnoid Hemorrhage
SDS-PAGE	SDS Polyacrylamide Gel Electrophoresis
SD	Standard Deviation
SH2	Src Homology 2
S6K1	Ribosomal Protein S6 Kinase (1)
SOCS	Suppressor of Cytokine Signaling
TBST	Tris-Buffered Saline with Tween 20
TEMED	Tetramethylethylenediamine
TGF-β	Transforming Growth Factor Beta
TNF-α	Tumor Necrosis Factor Alpha
Tris	Tris(hydroxymethyl)aminomethane
UPS	Ubiquitin-Proteasome System

8 REFERENCE

Aguirre, V., T. Uchida, L. Yenush, R. Davis, and M. F. White. 2000. 'The c-Jun NH(2)-terminal kinase promotes insulin resistance during association with insulin receptor substrate-1 and phosphorylation of Ser(307)', *J Biol Chem*, 275: 9047-54.

Anrather, J., and C. Iadecola. 2016. 'Inflammation and Stroke: An Overview', *Neurotherapeutics*, 13: 661-70.

Bai, Q. K., Z. G. Zhao, L. J. Lu, J. Shen, J. Y. Zhang, H. J. Sui, X. H. Xie, J. Chen, J. Yang, and C. R. Chen. 2019. 'Treating ischaemic stroke with intravenous tPA beyond 4.5 hours under the guidance of a MRI DWI/T2WI mismatch was safe and effective', *Stroke Vasc Neurol*, 4: 8-13.

Balami, J. S., G. Hadley, B. A. Sutherland, H. Karbalai, and A. M. Buchan. 2013. 'The exact science of stroke thrombolysis and the quiet art of patient selection', *Brain*, 136: 3528-53.

Barthels, D., and H. Das. 2020. 'Current advances in ischemic stroke research and therapies', *Biochim Biophys Acta Mol Basis Dis*, 1866: 165260.

Bjorkoy, G., T. Lamark, A. Brech, H. Outzen, M. Perander, A. Overvatn, H. Stenmark, and T. Johansen. 2005. 'p62/SQSTM1 forms protein aggregates degraded by autophagy and has a protective effect on huntingtin-induced cell death', *J Cell Biol*, 171: 603-14.

Burillo, J., P. Marqués, B. Jiménez, C. González-Blanco, M. Benito, and C. Guillén. 2021. 'Insulin Resistance and Diabetes Mellitus in Alzheimer's Disease', *Cells*, 10.

Carloni, S., G. Buonocore, and W. Balduini. 2008. 'Protective role of autophagy in neonatal hypoxia-ischemia induced brain injury', *Neurobiol Dis*, 32: 329-39.

Chakraborty, C., G. Agoramoorthy, and M. J. Hsu. 2011. 'Exploring the evolutionary relationship of insulin receptor substrate family using computational biology', *PLoS One*, 6: e16580.

Chamorro, A., U. Dirnagl, X. Urra, and A. M. Planas. 2016. 'Neuroprotection in acute stroke: targeting excitotoxicity, oxidative and nitrosative stress, and inflammation', *Lancet Neurol*, 15: 869-81.

Cherra, S. J., 3rd, and C. T. Chu. 2008. 'Autophagy in neuroprotection and neurodegeneration: A question of balance', *Future Neurol*, 3: 309-23.

Copps, K. D., and M. F. White. 2012. 'Regulation of insulin sensitivity by serine/threonine phosphorylation of insulin receptor substrate proteins IRS1 and IRS2', *Diabetologia*, 55: 2565-82.

Dai, S., Y. Feng, C. Lu, H. Zhang, W. Ma, W. Xie, X. Wu, P. Luo, L. Zhang, F. Fei, Z. Fei, and X. Li. 2024. 'Impairment of Autophagic Flux After Hypobaric Hypoxia Potentiates Oxidative Stress and Cognitive Function Disturbances in Mice', *Neurosci Bull*, 40: 35-49.

de Mello, N. P., A. M. Orellana, C. H. Mazucanti, G. de Morais Lima, C. Scavone, and E. M. Kawamoto. 2019. 'Insulin and Autophagy in Neurodegeneration', *Front Neurosci*, 13: 491.

Dhanoa, B. S., T. Cogliati, A. G. Satish, E. A. Bruford, and J. S. Friedman. 2013. 'Update on the Kelch-like (KLHL) gene family', *Hum Genomics*, 7: 13.

Donnan, G. A., M. Fisher, M. Macleod, and S. M. Davis. 2008. 'Stroke', *Lancet*, 371: 1612-23.

Durukan, A., and T. Tatlisumak. 2007. 'Acute ischemic stroke: overview of major experimental rodent models, pathophysiology, and therapy of focal cerebral ischemia', *Pharmacol Biochem Behav*, 87: 179-97.
Fath, T., Y. D. Ke, P. Gunning, J. Götz, and L. M. Ittner. 2009. 'Primary support cultures of hippocampal and substantia nigra neurons', *Nat Protoc*, 4: 78-85.
Frendo-Cumbo, S., J. R. Jaldin-Fincati, E. Coyaud, E. M. N. Laurent, L. K. Townsend, J. M. J. Tan, R. J. Xavier, N. J. Pillon, B. Raught, D. C. Wright, J. H. Brumell, and A. Klip. 2019. 'Deficiency of the autophagy gene ATG16L1 induces insulin resistance through KLHL9/KLHL13/CUL3-mediated IRS1 degradation', *J Biol Chem*, 294: 16172-85.
Frendo-Cumbo, Scott. 2021. *Identification of New IRS1 Interactors in the Regulation of Insulin Signalling and Cell Proliferation* (University of Toronto (Canada)).
Fu, J., L. Yu, Q. Yu, N. Yu, F. Xu, and S. Li. 2023. 'Ginsenoside compound K reduces ischemia/reperfusion-induced neuronal apoptosis by inhibiting PTP1B-mediated IRS1 tyrosine dephosphorylation', *J Ginseng Res*, 47: 274-82.
Galluzzi, L., J. M. Bravo-San Pedro, K. Blomgren, and G. Kroemer. 2016. 'Autophagy in acute brain injury', *Nat Rev Neurosci*, 17: 467-84.
Geetha, T., C. Zheng, N. Vishwaprakash, T. L. Broderick, and J. R. Babu. 2012. 'Sequestosome 1/p62, a scaffolding protein, is a newly identified partner of IRS-1 protein', *J Biol Chem*, 287: 29672-8.
Gil-Garcia, C. A., E. Flores-Alvarez, R. Cebrian-Garcia, A. C. Mendoza-Lopez, L. M. Gonzalez-Hermosillo, M. D. Garcia-Blanco, and E. Roldan-Valadez. 2022. 'Essential Topics About the Imaging Diagnosis and Treatment of Hemorrhagic Stroke: A Comprehensive Review of the 2022 AHA Guidelines', *Curr Probl Cardiol*, 47: 101328.
Gual, P., Y. Le Marchand-Brustel, and J. F. Tanti. 2005. 'Positive and negative regulation of insulin signaling through IRS-1 phosphorylation', *Biochimie*, 87: 99-109.
Hankey, G. J. 2013. 'The global and regional burden of stroke', *Lancet Glob Health*, 1: e239-40.
Harrington, L. S., G. M. Findlay, A. Gray, T. Tolkacheva, S. Wigfield, H. Rebholz, J. Barnett, N. R. Leslie, S. Cheng, P. R. Shepherd, I. Gout, C. P. Downes, and R. F. Lamb. 2004. 'The TSC1-2 tumor suppressor controls insulin-PI3K signaling via regulation of IRS proteins', *J Cell Biol*, 166: 213-23.
Hisham, N. F., and U. Bayraktutan. 2013. 'Epidemiology, pathophysiology, and treatment of hypertension in ischaemic stroke patients', *J Stroke Cerebrovasc Dis*, 22: e4-14.
Hotamisligil, G. S., P. Peraldi, A. Budavari, R. Ellis, M. F. White, and B. M. Spiegelman. 1996. 'IRS-1-mediated inhibition of insulin receptor tyrosine kinase activity in TNF-alpha- and obesity-induced insulin resistance', *Science*, 271: 665-8.
Huang, C. C., C. C. Lee, and K. S. Hsu. 2010. 'The role of insulin receptor signaling in synaptic plasticity and cognitive function', *Chang Gung Med J*, 33: 115-25.
Iadecola, C., M. S. Buckwalter, and J. Anrather. 2020. 'Immune responses to stroke: mechanisms, modulation, and therapeutic potential', *J Clin Invest*, 130: 2777-88.
'Identification of New IRS1 Interactors in the Regulation of Insulin Signalling and Cell Proliferation'.
Igawa, H., A. Kikuchi, H. Misu, K. A. Ishii, S. Kaneko, and T. Takamura. 2019. 'p62-mediated autophagy affects nutrition-dependent insulin receptor substrate 1 dynamics in 3T3-L1 preadipocytes', *J Diabetes Investig*, 10: 32-42.

Kaech, S., and G. Banker. 2006. 'Culturing hippocampal neurons', *Nat Protoc*, 1: 2406-15.
Kang, S. G., A. L. Brown, and J. H. Chung. 2007. 'Oxygen tension regulates the stability of insulin receptor substrate-1 (IRS-1) through caspase-mediated cleavage', *J Biol Chem*, 282: 6090-7.
Katagiri, S., K. Park, Y. Maeda, T. N. Rao, M. Khamaisi, Q. Li, H. Yokomizo, A. Mima, L. Lancerotto, A. Wagers, D. P. Orgill, and G. L. King. 2016. 'Overexpressing IRS1 in Endothelial Cells Enhances Angioblast Differentiation and Wound Healing in Diabetes and Insulin Resistance', *Diabetes*, 65: 2760-71.
Katan, M., and A. Luft. 2018. 'Global Burden of Stroke', *Semin Neurol*, 38: 208-11.
Kim, J. A., M. Montagnani, K. K. Koh, and M. J. Quon. 2006. 'Reciprocal relationships between insulin resistance and endothelial dysfunction: molecular and pathophysiological mechanisms', *Circulation*, 113: 1888-904.
Kleinridders, A., H. A. Ferris, W. Cai, and C. R. Kahn. 2014. 'Insulin action in brain regulates systemic metabolism and brain function', *Diabetes*, 63: 2232-43.
Koepsell, H. 2020. 'Glucose transporters in brain in health and disease', *Pflugers Arch*, 472: 1299-343.
Kraft, C., M. Peter, and K. Hofmann. 2010. 'Selective autophagy: ubiquitin-mediated recognition and beyond', *Nat Cell Biol*, 12: 836-41.
Kristian, T. 2004. 'Metabolic stages, mitochondria and calcium in hypoxic/ischemic brain damage', *Cell Calcium*, 36: 221-33.
Kuang, Y., X. Zheng, L. Zhang, X. Ai, V. Venkataramani, E. Kilic, D. M. Hermann, A. Majid, M. Bähr, and T. R. Doeppner. 2020. 'Adipose-derived mesenchymal stem cells reduce autophagy in stroke mice by extracellular vesicle transfer of miR-25', *J Extracell Vesicles*, 10: e12024.
Kunz, A., U. Dirnagl, and P. Mergenthaler. 2010. 'Acute pathophysiological processes after ischaemic and traumatic brain injury', *Best Pract Res Clin Anaesthesiol*, 24: 495-509.
Laplante, M., and D. M. Sabatini. 2012. 'mTOR signaling in growth control and disease', *Cell*, 149: 274-93.
Lee, C. C., Y. M. Kuo, C. C. Huang, and K. S. Hsu. 2009. 'Insulin rescues amyloid beta-induced impairment of hippocampal long-term potentiation', *Neurobiol Aging*, 30: 377-87.
Li, G., E. J. Barrett, M. O. Barrett, W. Cao, and Z. Liu. 2007. 'Tumor necrosis factor-alpha induces insulin resistance in endothelial cells via a p38 mitogen-activated protein kinase-dependent pathway', *Endocrinology*, 148: 3356-63.
Li, S., A. Hafeez, F. Noorulla, X. Geng, G. Shao, C. Ren, G. Lu, H. Zhao, Y. Ding, and X. Ji. 2017. 'Preconditioning in neuroprotection: From hypoxia to ischemia', *Prog Neurobiol*, 157: 79-91.
Liu, F., J. Lu, A. Manaenko, J. Tang, and Q. Hu. 2018. 'Mitochondria in Ischemic Stroke: New Insight and Implications', *Aging Dis*, 9: 924-37.
Liu, J., X. Yi, Y. Tao, Y. Wang, and Z. Xu. 2020. 'Insulin-receptor substrate 1 protects against injury in endothelial cell models of ox-LDL-induced atherosclerosis by inhibiting ER stress/oxidative stress-mediated apoptosis and activating the Akt/FoxO1 signaling pathway', *Int J Mol Med*, 46: 1671-82.
Majumder, D. 2024. 'Ischemic Stroke: Pathophysiology and Evolving Treatment Approaches', *Neurosci Insights*, 19: 26331055241292600.

Martínez Báez, A., G. Ayala, A. Pedroza-Saavedra, H. M. González-Sánchez, and L. Chihu Amparan. 2024. 'Phosphorylation Codes in IRS-1 and IRS-2 Are Associated with the Activation/Inhibition of Insulin Canonical Signaling Pathways', *Curr Issues Mol Biol*, 46: 634-49.

Mayer, C. M., and D. D. Belsham. 2010. 'Central insulin signaling is attenuated by long-term insulin exposure via insulin receptor substrate-1 serine phosphorylation, proteasomal degradation, and lysosomal insulin receptor degradation', *Endocrinology*, 151: 75-84.

Milstein, J. L., and H. A. Ferris. 2021. 'The brain as an insulin-sensitive metabolic organ', *Mol Metab*, 52: 101234.

Moon, S., M. S. Chang, S. H. Koh, and Y. K. Choi. 2021. 'Repair Mechanisms of the Neurovascular Unit after Ischemic Stroke with a Focus on VEGF', *Int J Mol Sci*, 22.

Morino, K., S. Neschen, S. Bilz, S. Sono, D. Tsirigotis, R. M. Reznick, I. Moore, Y. Nagai, V. Samuel, D. Sebastian, M. White, W. Philbrick, and G. I. Shulman. 2008. 'Muscle-specific IRS-1 Ser->Ala transgenic mice are protected from fat-induced insulin resistance in skeletal muscle', *Diabetes*, 57: 2644-51.

Muthaian, R., G. Minhas, and A. Anand. 2012. 'Pathophysiology of stroke and stroke-induced retinal ischemia: emerging role of stem cells', *J Cell Physiol*, 227: 1269-79.

Nakao, R., K. Hirasaka, J. Goto, K. Ishidoh, C. Yamada, A. Ohno, Y. Okumura, I. Nonaka, K. Yasutomo, K. M. Baldwin, E. Kominami, A. Higashibata, K. Nagano, K. Tanaka, N. Yasui, E. M. Mills, S. Takeda, and T. Nikawa. 2009. 'Ubiquitin ligase Cbl-b is a negative regulator for insulin-like growth factor 1 signaling during muscle atrophy caused by unloading', *Mol Cell Biol*, 29: 4798-811.

Nystrom, F. H., and M. J. Quon. 1999. 'Insulin signalling: metabolic pathways and mechanisms for specificity', *Cell Signal*, 11: 563-74.

Pankiv, S., T. H. Clausen, T. Lamark, A. Brech, J. A. Bruun, H. Outzen, A. Overvatn, G. Bjorkoy, and T. Johansen. 2007. 'p62/SQSTM1 binds directly to Atg8/LC3 to facilitate degradation of ubiquitinated protein aggregates by autophagy', *J Biol Chem*, 282: 24131-45.

Pham-Huy, L. A., H. He, and C. Pham-Huy. 2008. 'Free radicals, antioxidants in disease and health', *Int J Biomed Sci*, 4: 89-96.

Qin, C., S. Yang, Y. H. Chu, H. Zhang, X. W. Pang, L. Chen, L. Q. Zhou, M. Chen, D. S. Tian, and W. Wang. 2022. 'Signaling pathways involved in ischemic stroke: molecular mechanisms and therapeutic interventions', *Signal Transduct Target Ther*, 7: 215.

Rui, L., M. Yuan, D. Frantz, S. Shoelson, and M. F. White. 2002. 'SOCS-1 and SOCS-3 block insulin signaling by ubiquitin-mediated degradation of IRS1 and IRS2', *J Biol Chem*, 277: 42394-8.

Runwal, G., E. Stamatakou, F. H. Siddiqi, C. Puri, Y. Zhu, and D. C. Rubinsztein. 2019. 'LC3-positive structures are prominent in autophagy-deficient cells', *Sci Rep*, 9: 10147.

Ryou, M. G., and R. T. Mallet. 2018. 'An In Vitro Oxygen-Glucose Deprivation Model for Studying Ischemia-Reperfusion Injury of Neuronal Cells', *Methods Mol Biol*, 1717: 229-35.

Saltiel, A. R., and C. R. Kahn. 2001. 'Insulin signalling and the regulation of glucose and lipid metabolism', *Nature*, 414: 799-806.

Sarbassov, D. D., D. A. Guertin, S. M. Ali, and D. M. Sabatini. 2005. 'Phosphorylation and regulation of Akt/PKB by the rictor-mTOR complex', *Science*, 307: 1098-101.
Schinner, S., W. A. Scherbaum, S. R. Bornstein, and A. Barthel. 2005. 'Molecular mechanisms of insulin resistance', *Diabet Med*, 22: 674-82.
Schulingkamp, R. J., T. C. Pagano, D. Hung, and R. B. Raffa. 2000. 'Insulin receptors and insulin action in the brain: review and clinical implications', *Neurosci Biobehav Rev*, 24: 855-72.
Sedaghat, A. R., A. Sherman, and M. J. Quon. 2002. 'A mathematical model of metabolic insulin signaling pathways', *Am J Physiol Endocrinol Metab*, 283: E1084-101.
Sekar, S., and C. Taghibiglou. 2018. 'Elevated nuclear phosphatase and tensin homolog (PTEN) and altered insulin signaling in substantia nigral region of patients with Parkinson's disease', *Neurosci Lett*, 666: 139-43.
Shaw, L. M. 2011. 'The insulin receptor substrate (IRS) proteins: at the intersection of metabolism and cancer', *Cell Cycle*, 10: 1750-6.
Shen, Z., M. Xiang, C. Chen, F. Ding, Y. Wang, C. Shang, L. Xin, Y. Zhang, and X. Cui. 2022. 'Glutamate excitotoxicity: Potential therapeutic target for ischemic stroke', *Biomed Pharmacother*, 151: 113125.
Sun, M. S., H. Jin, X. Sun, S. Huang, F. L. Zhang, Z. N. Guo, and Y. Yang. 2018. 'Free Radical Damage in Ischemia-Reperfusion Injury: An Obstacle in Acute Ischemic Stroke after Revascularization Therapy', *Oxid Med Cell Longev*, 2018: 3804979.
Tanti, J. F., T. Gremeaux, E. van Obberghen, and Y. Le Marchand-Brustel. 1994. 'Serine/threonine phosphorylation of insulin receptor substrate 1 modulates insulin receptor signaling', *J Biol Chem*, 269: 6051-7.
Tanti, J. F., and J. Jager. 2009. 'Cellular mechanisms of insulin resistance: role of stress-regulated serine kinases and insulin receptor substrates (IRS) serine phosphorylation', *Curr Opin Pharmacol*, 9: 753-62.
Tramutola, A., J. C. Triplett, F. Di Domenico, D. M. Niedowicz, M. P. Murphy, R. Coccia, M. Perluigi, and D. A. Butterfield. 2015. 'Alteration of mTOR signaling occurs early in the progression of Alzheimer disease (AD): analysis of brain from subjects with pre-clinical AD, amnestic mild cognitive impairment and late-stage AD', *J Neurochem*, 133: 739-49.
Tremblay, F., S. Brûlé, S. Hee Um, Y. Li, K. Masuda, M. Roden, X. J. Sun, M. Krebs, R. D. Polakiewicz, G. Thomas, and A. Marette. 2007. 'Identification of IRS-1 Ser-1101 as a target of S6K1 in nutrient- and obesity-induced insulin resistance', *Proc Natl Acad Sci U S A*, 104: 14056-61.
Tsao, C. W., A. W. Aday, Z. I. Almarzooq, C. A. M. Anderson, P. Arora, C. L. Avery, C. M. Baker-Smith, A. Z. Beaton, A. K. Boehme, A. E. Buxton, Y. Commodore-Mensah, M. S. V. Elkind, K. R. Evenson, C. Eze-Nliam, S. Fugar, G. Generoso, D. G. Heard, S. Hiremath, J. E. Ho, R. Kalani, D. S. Kazi, D. Ko, D. A. Levine, J. Liu, J. Ma, J. W. Magnani, E. D. Michos, M. E. Mussolino, S. D. Navaneethan, N. I. Parikh, R. Poudel, M. Rezk-Hanna, G. A. Roth, N. S. Shah, M. P. St-Onge, E. L. Thacker, S. S. Virani, J. H. Voeks, N. Y. Wang, N. D. Wong, S. S. Wong, K. Yaffe, S. S. Martin, Epidemiology American Heart Association Council on, Committee Prevention Statistics, and Subcommittee Stroke Statistics. 2023. 'Heart Disease and Stroke Statistics-2023 Update: A Report From the American Heart Association', *Circulation*, 147: e93-e621.
Tu, Y. F., S. T. Jiang, C. W. Chiang, L. C. Chen, and C. C. Huang. 2021. 'Endothelial-specific insulin receptor substrate-1 overexpression worsens neonatal hypoxic-

ischemic brain injury via mTOR-mediated tight junction disassembly', *Cell Death Discov*, 7: 150.
Tu, Y. F., S. T. Jiang, Y. H. Chow, C. C. Huang, C. J. Ho, and Y. P. Chou. 2016. 'Insulin Receptor Substrate-1 Activation Mediated p53 Downregulation Protects Against Hypoxic-Ischemia in the Neonatal Brain', *Mol Neurobiol*, 53: 3658-69.
Turnbull, A., H. T. Wang, C. Murphy, N. S. P. Ho, X. Wang, M. Sormaz, T. Karapanagiotidis, R. M. Leech, B. Bernhardt, D. S. Margulies, D. Vatansever, E. Jefferies, and J. Smallwood. 2019. 'Left dorsolateral prefrontal cortex supports context-dependent prioritisation of off-task thought', *Nat Commun*, 10: 3816.
Tzatsos, A., and K. V. Kandror. 2006. 'Nutrients suppress phosphatidylinositol 3-kinase/Akt signaling via raptor-dependent mTOR-mediated insulin receptor substrate 1 phosphorylation', *Mol Cell Biol*, 26: 63-76.
van der Heide, L. P., A. Kamal, A. Artola, W. H. Gispen, and G. M. Ramakers. 2005. 'Insulin modulates hippocampal activity-dependent synaptic plasticity in a N-methyl-d-aspartate receptor and phosphatidyl-inositol-3-kinase-dependent manner', *J Neurochem*, 94: 1158-66.
Veno, S. K., E. B. Schmidt, and C. S. Bork. 2019. 'Polyunsaturated Fatty Acids and Risk of Ischemic Stroke', *Nutrients*, 11.
Verma, M., B. N. Lizama, and C. T. Chu. 2022. 'Excitotoxicity, calcium and mitochondria: a triad in synaptic neurodegeneration', *Transl Neurodegener*, 11: 3.
Wafa, H. A., C. D. A. Wolfe, E. Emmett, G. A. Roth, C. O. Johnson, and Y. Wang. 2020. 'Burden of Stroke in Europe: Thirty-Year Projections of Incidence, Prevalence, Deaths, and Disability-Adjusted Life Years', *Stroke*, 51: 2418-27.
Wainszelbaum, M. J., J. Liu, C. Kong, P. Srikanth, D. Samovski, X. Su, and P. D. Stahl. 2012. 'TBC1D3, a hominoid-specific gene, delays IRS-1 degradation and promotes insulin signaling by modulating p70 S6 kinase activity', *PLoS One*, 7: e31225.
White, M. F. 1997. 'The insulin signalling system and the IRS proteins', *Diabetologia*, 40 Suppl 2: S2-17.
Xu, X., M. Keshwani, K. Meyer, A. Sarikas, S. Taylor, and Z. Q. Pan. 2012. 'Identification of the degradation determinants of insulin receptor substrate 1 for signaling cullin-RING E3 ubiquitin ligase 7-mediated ubiquitination', *J Biol Chem*, 287: 40758-66.
Xu, X., A. Sarikas, D. C. Dias-Santagata, G. Dolios, P. J. Lafontant, S. C. Tsai, W. Zhu, H. Nakajima, H. O. Nakajima, L. J. Field, R. Wang, and Z. Q. Pan. 2008. 'The CUL7 E3 ubiquitin ligase targets insulin receptor substrate 1 for ubiquitin-dependent degradation', *Mol Cell*, 30: 403-14.
Yang, J., M. D. C. Vitery, J. Chen, J. Osei-Owusu, J. Chu, and Z. Qiu. 2019. 'Glutamate-Releasing SWELL1 Channel in Astrocytes Modulates Synaptic Transmission and Promotes Brain Damage in Stroke', *Neuron*, 102: 813-27 e6.
Yoneyama, Y., T. Inamitsu, K. Chida, S. I. Iemura, T. Natsume, T. Maeda, F. Hakuno, and S. I. Takahashi. 2018. 'Serine Phosphorylation by mTORC1 Promotes IRS-1 Degradation through SCFβ-TRCP E3 Ubiquitin Ligase', *iScience*, 5: 1-18.
Zang, L., D. Fu, F. Zhang, N. Li, and X. Ma. 2023. 'Tenuigenin activates the IRS1/Akt/mTOR signaling by blocking PTPN1 to inhibit autophagy and improve locomotor recovery in spinal cord injury', *J Ethnopharmacol*, 317: 116841.
Zhang, J., Z. Gao, J. Yin, M. J. Quon, and J. Ye. 2008. 'S6K directly phosphorylates IRS-1 on Ser-270 to promote insulin resistance in response to TNF-(alpha) signaling through IKK2', *J Biol Chem*, 283: 35375-82.

Zhang, L., W. Wei, X. Ai, E. Kilic, D. M. Hermann, V. Venkataramani, M. Bähr, and T. R. Doeppner. 2021. 'Extracellular vesicles from hypoxia-preconditioned microglia promote angiogenesis and repress apoptosis in stroke mice via the TGF-β/Smad2/3 pathway', *Cell Death Dis*, 12: 1068.

Zhao, Y., X. Zhang, X. Chen, and Y. Wei. 2022. 'Neuronal injuries in cerebral infarction and ischemic stroke: From mechanisms to treatment (Review)', *Int J Mol Med*, 49.

Zheng, M., and P. Wang. 2021. 'Role of insulin receptor substance-1 modulating PI3K/Akt insulin signaling pathway in Alzheimer's disease', *3 Biotech*, 11: 179.

Zhu, J., Y. Wan, H. Xu, Y. Wu, B. Hu, and H. Jin. 2019. 'The role of endogenous tissue-type plasminogen activator in neuronal survival after ischemic stroke: friend or foe?', *Cell Mol Life Sci*, 76: 1489-506.

Zhu, W., X. He, D. Huang, Y. Jiang, W. Hong, S. Ke, E. Wang, F. Wang, X. Wang, R. Shan, S. Liu, Y. Xu, and Y. Jiang. 2024. 'Global and Regional Burden of Ischemic Stroke Disease from 1990 to 2021: An Age-Period-Cohort Analysis', *Transl Stroke Res*.

9 EHRENWÖRTLICHE ERKLÄRUNG

„Hiermit erkläre ich, dass ich die vorliegende Arbeit selbständig und ohne unzulässige Hilfe oder Benutzung anderer als der angegebenen Hilfsmittel angefertigt habe. Alle Textstellen, die wörtlich oder sinngemäß aus veröffentlichten oder nichtveröffentlichten Schriften entnommen sind, und alle Angaben, die auf mündlichen Auskünften beruhen, sind als solche kenntlich gemacht. Bei den von mir durchgeführten und in der Dissertation erwähnten Untersuchungen habe ich die Grundsätze guter wissenschaftlicher Praxis, wie sie in der „Satzung der Justus-Liebig-Universität Gießen zur Sicherung guter wissenschaftlicher Praxis“ niedergelegt sind, eingehalten sowie ethische, datenschutzrechtliche und tierschutzrechtliche Grundsätze befolgt. Ich versichere, dass Dritte von mir weder unmittelbar noch mittelbar geldwerte Leistungen für Arbeiten erhalten haben, die im Zusammenhang mit dem Inhalt der vorgelegten Dissertation stehen, und dass die vorgelegte Arbeit weder im Inland noch im Ausland in gleicher oder ähnlicher Form einer anderen Prüfungsbehörde zum Zweck einer Promotion oder eines anderen Prüfungsverfahrens vorgelegt wurde. Alles aus anderen Quellen und von anderen Personen übernommene Material, das in der Arbeit verwendet wurde oder auf das direkt Bezug genommen wird, wurde als solches kenntlich gemacht. Insbesondere wurden alle Personen genannt, die direkt und indirekt an der Entstehung der vorliegenden Arbeit beteiligt waren. Mit der Überprüfung meiner Arbeit durch eine Plagiatserkennungssoftware bzw. ein internetbasiertes Softwareprogramm erkläre ich mich einverstanden.“

_____ _____

Ort/Datum Unterschrift

10 AKNOWLEDGEMENT

First of all, I am deeply grateful to have met so many kind and friendly people in Germany. Although we come from all over the world, we have shared countless wonderful moments over the past three years, which will remain a lifelong treasure for me.

My most sincere and heartfelt thanks go first to my supervisor, Professor Thorsten Roland Döppner, who gave me the opportunity to further explore the field of scientific research and helped me develop scientific thinking and problem-solving abilities. I would also like to express my special thanks to the postdoctoral researchers Dr. Sabine Huber and Dr. Samir Vaid, who guided me in experimental techniques and helped me overcome various challenges I encountered during my experiments.

I am truly grateful to all my colleagues and friends, who have been my emotional support throughout this journey. I deeply appreciate and cherish the opportunity to study at Justus Liebig University Giessen.

Last but most importantly, I would like to express my heartfelt gratitude to my beloved family for their unconditional support, trust, and faith in me. Thank you for always being there for me.